Because of the close association of the cascade downstream of ADAR2 downregulation to ALS pathogenesis, enhancement of deficient ADAR2 in the motor neurons to a level sufficient to edit the GluA2 Q/R site may be a logical new therapy for sporadic ALS and the normalization of TDP-43 nuclear localization would be a biomarker for the therapeutic effects in the model animals (Yamashita et al., 2013).

Acknowledgments

This study was supported in part by Grants-in-Aid for Scientific Research from the Ministry of Health, Labour and Welfare of Japan to S.K. (H21-Kokoro-017) and from the Ministry of Education, Culture, Sports, Science and Technology of Japan to T.Y. (19790601 and 23790977) and S.K. (19390235 and 22390173).

REFERENCES

Aizawa, H., et al., 2010. TDP-43 pathology in sporadic ALS occurs in motor neurons lacking the RNA editing enzyme ADAR2. Acta Neuropathol. 120, 75–84.

Arai, T., et al., 2006. TDP-43 is a component of ubiquitin-positive tau-negative inclusions in frontotemporal lobar degeneration and amyotrophic lateral sclerosis. Biochem. Biophys. Res. Commun. 351, 602–611.

Brusa, R., et al., 1995. Early-onset epilepsy and postnatal lethality associated with an editing-deficient GluR-B allele in mice. Science 270, 1677–1680.

Buratti, E., Baralle, F.E., 2010. The multiple roles of TDP-43 in pre-mRNA processing and gene expression regulation. RNA Biol. 7, 420–429.

Carriedo, S.G., Yin, H.Z., Weiss, J.H., 1996. Motor neurons are selectively vulnerable to AMPA/kainate receptor-mediated injury *in vitro*. J. Neurosci. 16, 4069–4079.

Cattenoz, P.B., et al., 2013. Transcriptome-wide identification of A>I RNA editing sites by inosine specific cleavage. RNA 19, 257–270.

Chen-Plotkin, A.S., Lee, V.M., Trojanowski, J.Q., 2010. TAR DNA-binding protein 43 in neurodegenerative disease. Nat. Rev. Neurol. 6, 211–220.

Chen, C.X., et al., 2000. A third member of the RNA-specific adenosine deaminase gene family, ADAR3, contains both single- and double-stranded RNA binding domains. RNA 6, 755–767.

Colombrita, C., et al., 2012. TDP-43 and FUS RNA-binding proteins bind distinct sets of cytoplasmic messenger RNAs and differently regulate their post-transcriptional fate in motoneuron-like cells. J. Biol. Chem. 287, 15635–15647.

Daoud, H., et al., 2009. Contribution of TARDBP mutations to sporadic amyotrophic lateral sclerosis. J. Med. Genet. 46, 112–114.

DeJesus-Hernandez, M., et al., 2011. Expanded GGGGCC hexanucleotide repeat in noncoding region of C9ORF72 causes chromosome 9p-linked FTD and ALS. Neuron 72, 245–256.

Donnelly, C.J., et al., 2013. RNA toxicity from the ALS/FTD C9ORF72 expansion is mitigated by antisense intervention. Neuron 80, 415–428.

Dormann, D., et al., 2009. Proteolytic processing of TAR DNA binding protein-43 by caspases produces C-terminal fragments with disease defining properties independent of progranulin. J. Neurochem. 110, 1082–1094.

Feldmeyer, D., et al., 1999. Neurological dysfunctions in mice expressing different levels of the Q/R site-unedited AMPAR subunit GluR-B. Nat. Neurosci. 2, 57–64.

Ferraiuolo, L., et al., 2011. Molecular pathways of motor neuron injury in amyotrophic lateral sclerosis. Nat. Rev. Neurol. 7, 616–630.

Flomen, R., Makoff, A., 2011. Increased RNA editing in EAAT2 pre-mRNA from amyotrophic lateral sclerosis patients: involvement of a cryptic polyadenylation site. Neurosci. Lett. 497, 139–143.

Garncarz, W., et al., 2013. A high-throughput screen to identify enhancers of ADAR-mediated RNA-editing. RNA Biol. 10, 192–204.

Gendron, T.F., Petrucelli, L., 2011. Rodent models of TDP-43 proteinopathy: investigating the mechanisms of TDP-43-mediated neurodegeneration. J. Mol. Neurosci. 45, 486–499.

Gendron, T.F., et al., 2013. Antisense transcripts of the expanded C9ORF72 hexanucleotide repeat form nuclear RNA foci and undergo repeat-associated non-ATG translation in c9FTD/ALS. Acta Neuropathol. 126, 829–844.

Geser, F., et al., 2010. Pathological 43-kDa transactivation response DNA-binding protein in older adults with and without severe mental illness. Arch. Neurol. 67, 1238–1250.

Gitcho, M.A., et al., 2008. TDP-43 A315T mutation in familial motor neuron disease. Ann. Neurol. 63, 535–538.

Hasegawa, M., et al., 2008. Phosphorylated TDP-43 in frontotemporal lobar degeneration and amyotrophic lateral sclerosis. Ann. Neurol. 64, 60–70.

Herskowitz, J.H., et al., 2012. Asparaginyl endopeptidase cleaves TDP-43 in brain. Proteomics 12, 2455–2463.

Hideyama, T., et al., 2010. Induced loss of ADAR2 engenders slow death of motor neurons from Q/R site-unedited GluR2. J. Neurosci. 30, 11917–11925.

Hideyama, T., Kwak, S., 2011. When does ALS start? ADAR2-GluA2 hypothesis for the etiology of sporadic ALS. Front. Mol. Neurosci. 4, 33.

Hideyama, T., et al., 2012a. Co-Occurrence of TDP-43 mislocalization with reduced activity of an RNA editing enzyme, ADAR2, in aged mouse motor neurons. PLoS One 7, e43469.

Hideyama, T., et al., 2012b. Profound downregulation of the RNA editing enzyme ADAR2 in ALS spinal motor neurons. Neurobiol. Dis. 45, 1121–1128.

Higuchi, M., et al., 2000. Point mutation in an AMPA receptor gene rescues lethality in mice deficient in the RNA-editing enzyme ADAR2. Nature 406, 78–81.

Hogg, M., et al., 2011. RNA editing by mammalian ADARs. Adv. Genet. 73, 87–120.

Igaz, L.M., et al., 2009. Expression of TDP-43 C-terminal fragments *in Vitro* recapitulates pathological features of TDP-43 proteinopathies. J. Biol. Chem. 284, 8516–8524.

Iguchi, Y., et al., 2009. TDP-43 depletion induces neuronal cell damage through dysregulation of Rho family GTPases. J. Biol. Chem. 284, 22059–22066.

Jiang, Y.M., et al., 2005. Gene expression profile of spinal motor neurons in sporadic amyotrophic lateral sclerosis. Ann. Neurol. 57, 236–251.

Johnson, B.S., et al., 2009. TDP-43 is intrinsically aggregation-prone, and amyotrophic lateral sclerosis-linked mutations accelerate aggregation and increase toxicity. J. Biol. Chem. 284, 20329–20339.

Kabashi, E., et al., 2008. TARDBP mutations in individuals with sporadic and familial amyotrophic lateral sclerosis. Nat. Genet. 40, 572–574.

Kanazawa, M., et al., 2011. Biochemical and histopathological alterations in TAR DNA-binding protein-43 after acute ischemic stroke in rats. J. Neurochem. 116, 957–965.

Kask, K., et al., 1998. The AMPA receptor subunit GluR-B in its Q/R site-unedited form is not essential for brain development and function. Proc. Natl. Acad. Sci. USA 95, 13777–13782.

Kawahara, Y., et al., 2003. Human spinal motoneurons express low relative abundance of GluR2 mRNA: an implication for excitotoxicity in ALS. J. Neurochem. 85, 680–689.
Kawahara, Y., et al., 2004. Glutamate receptors: RNA editing and death of motor neurons. Nature 427, 801.
Kawahara, Y., et al., 2006. Underediting of GluR2 mRNA, a neuronal death inducing molecular change in sporadic ALS, does not occur in motor neurons in ALS1 or SBMA. Neurosci. Res. 54, 11–14.
Kim, H.J., et al., 2013. Mutations in prion-like domains in hnRNPA2B1 and hnRNPA1 cause multisystem proteinopathy and ALS. Nature 495, 467–473.
Kwak, S., Kawahara, Y., 2005. Deficient RNA editing of GluR2 and neuronal death in amyotropic lateral sclerosis. J. Mol. Med. 83, 110–120.
Kwiatkowski Jr., T.J., et al., 2009. Mutations in the FUS/TLS gene on chromosome 16 cause familial amyotrophic lateral sclerosis. Science 323, 1205–1208.
Lagier-Tourenne, C., Polymenidou, M., Cleveland, D.W., 2010. TDP-43 and FUS/TLS: emerging roles in RNA processing and neurodegeneration. Hum. Mol. Genet. 19, R46–R64.
Lagier-Tourenne, C., et al., 2013. Targeted degradation of sense and antisense C9orf72 RNA foci as therapy for ALS and frontotemporal degeneration. Proc. Natl. Acad. Sci. USA 110, E4530–E4539.
Li, J.B., et al., 2009. Genome-wide identification of human RNA editing sites by parallel DNA capturing and sequencing. Science 324, 1210–1213.
Li, X., et al., 2013. The ADAR RNA editing enzyme controls neuronal excitability in *Drosophila melanogaster*. Nucleic Acids Res.
Lopatniuk, P., Witkowski, J.M., 2011. Conventional calpains and programmed cell death. Acta Biochim. Pol. 58, 287–296.
Maas, S., et al., 2011. Genome-wide evaluation and discovery of vertebrate A-to-I RNA editing sites. Biochem. Biophys. Res. Commun. 412, 407–412.
Mackenzie, I.R., et al., 2007. Pathological TDP-43 distinguishes sporadic amyotrophic lateral sclerosis from amyotrophic lateral sclerosis with SOD1 mutations. Ann. Neurol. 61, 427–434.
McKee, A.C., et al., 2010. TDP-43 proteinopathy and motor neuron disease in chronic traumatic encephalopathy. J. Neuropathol. Exp. Neurol. 69, 918–929.
Melcher, T., et al., 1996. A mammalian RNA editing enzyme. Nature 379, 460–464.
Moisse, K., et al., 2009. Divergent patterns of cytosolic TDP-43 and neuronal progranulin expression following axotomy: implications for TDP-43 in the physiological response to neuronal injury. Brain Res. 1249, 202–211.
Neumann, M., et al., 2006. Ubiquitinated TDP-43 in frontotemporal lobar degeneration and amyotrophic lateral sclerosis. Science 314, 130–133.
Nishimoto, Y., et al., 2009. Characterization of alternative isoforms and inclusion body of the TAR DNA binding protein-43. J. Biol. Chem.
Nishimoto, Y., et al., 2013. The long non-coding RNA nuclear-enriched abundant transcript 1_2 induces paraspeckle formation in the motor neuron during the early phase of amyotrophic lateral sclerosis. Mol. Brain 6, 31.
Nonaka, T., et al., 2009. Truncation and pathogenic mutations facilitate the formation of intracellular aggregates of TDP-43. Hum. Mol. Genet. 18, 3353–3364.
Peng, Z., et al., 2012. Comprehensive analysis of RNA-Seq data reveals extensive RNA editing in a human transcriptome. Nat. Biotechnol. 30, 253–260.
Polymenidou, M., et al., 2011. Long pre-mRNA depletion and RNA missplicing contribute to neuronal vulnerability from loss of TDP-43. Nat. Neurosci. 14, 459–468.
Rademakers, R., van Blitterswijk, M., 2013. Motor neuron disease in 2012: novel causal genes and disease modifiers. Nat. Rev. Neurol. 9, 63–64.
Renton, A.E., et al., 2011. A hexanucleotide repeat expansion in C9ORF72 is the cause of chromosome 9p21-linked ALS-FTD. Neuron 72, 257–268.
Robertson, J., et al., 2007. Lack of TDP-43 abnormalities in mutant SOD1 transgenic mice shows disparity with ALS. Neurosci. Lett. 420, 128–132.
Rosen, D.R., et al., 1993. Mutations in Cu/Zn superoxide dismutase gene are associated with familial amyotrophic lateral sclerosis. Nature 362, 59–62.
Sareen, D., et al., 2013. Targeting RNA foci in iPSC-derived motor neurons from ALS patients with a C9ORF72 repeat expansion. Sci. Transl. Med. 5 (208ra149).
Seeburg, P.H., 2002. A-to-I editing: new and old sites, functions and speculations. Neuron 35, 17–20.
Sephton, C.F., et al., 2011. Identification of neuronal RNA targets of TDP-43-containing ribonucleoprotein complexes. J. Biol. Chem. 286, 1204–1215.
Solomon, O., et al., 2013. Global regulation of alternative splicing by adenosine deaminase acting on RNA (ADAR). RNA 19, 591–604.
Sommer, B., et al., 1991. RNA editing in brain controls a determinant of ion flow in glutamate-gated channels. Cell 67, 11–19.
Sreedharan, J., et al., 2008. TDP-43 mutations in familial and sporadic amyotrophic lateral sclerosis. Science 319, 1668–1672.
Sun, H., et al., 2005. Expression profile of AMPA receptor subunit mRNA in single adult rat brain and spinal cord neurons *in situ*. Neurosci. Res. 52, 228–234.
Takano, J., et al., 2005. Calpain mediates excitotoxic DNA fragmentation via mitochondrial pathways in adult brains: evidence from calpastatin mutant mice. J. Biol. Chem. 280, 16175–16184.
Takuma, H., et al., 1999. Reduction of GluR2 RNA editing, a molecular change that increases calcium influx through AMPA receptors, selective in the spinal ventral gray of patients with amyotrophic lateral sclerosis. Ann. Neurol. 46, 806–815.
Tan, C.F., et al., 2007. TDP-43 immunoreactivity in neuronal inclusions in familial amyotrophic lateral sclerosis with or without SOD1 gene mutation. Acta Neuropathol. 113, 535–542.
Tollervey, J.R., et al., 2011. Characterizing the RNA targets and position-dependent splicing regulation by TDP-43. Nat. Neurosci. 14, 452–458.
Van Deerlin, V.M., et al., 2008. TARDBP mutations in amyotrophic lateral sclerosis with TDP-43 neuropathology: a genetic and histopathological analysis. Lancet Neurol. 7, 409–416.
Vance, C., et al., 2009. Mutations in FUS, an RNA processing protein, cause familial amyotrophic lateral sclerosis type 6. Science 323, 1208–1211.
Wilson, A.C., et al., 2011. TDP-43 in aging and Alzheimer's disease – a review. Int. J. Clin. Exp. Pathol. 4, 147–155.
Yamashita, T., et al., 2012a. A role for calpain-dependent cleavage of TDP-43 in amyotrophic lateral sclerosis pathology. Nat. Commun. 3, 1307.
Yamashita, T., et al., 2012b. The abnormal processing of TDP-43 is not an upstream event of reduced ADAR2 activity in ALS motor neurons. Neurosci. Res. 73, 153–160.
Yamashita, T., et al., 2013. Rescue of amyotrophic lateral sclerosis phenotype in a mouse model by intravenous AAV9-ADAR2 delivery to motor neurons. EMBO Mol. Med. 5, 1710–1719.
Yokoseki, A., et al., 2008. TDP-43 mutation in familial amyotrophic lateral sclerosis. Ann. Neurol. 63, 538–542.

Zhang, Y.J., et al., 2007. Progranulin mediates caspase-dependent cleavage of TAR DNA binding protein-43. J. Neurosci. 27, 10530–10534.
Zhang, Y.J., et al., 2009. Aberrant cleavage of TDP-43 enhances aggregation and cellular toxicity. Proc. Natl. Acad. Sci. USA 106, 7607–7612.
Zhu, S., et al., 2013. Prediction of constitutive A-to-I editing sites from human transcriptomes in the absence of genomic sequences. BMC Genom. 14, 206.
Zu, T., et al., 2013. RAN proteins and RNA foci from antisense transcripts in C9ORF72 ALS and frontotemporal dementia. Proc. Natl. Acad. Sci. USA.

nature COMMUNICATIONS

ARTICLE

Received 1 May 2014 | Accepted 18 Dec 2014 | Published 20 Jan 2015

DOI: 10.1038/ncomms7116 OPEN

The unexpected role of polyubiquitin chains in the formation of fibrillar aggregates

Daichi Morimoto[1], Erik Walinda[1], Harumi Fukada[2], Yu-Shin Sou[3], Shun Kageyama[3,4], Masaru Hoshino[5], Takashi Fujii[6], Hikaru Tsuchiya[7], Yasushi Saeki[7], Kyohei Arita[8], Mariko Ariyoshi[1], Hidehito Tochio[9], Kazuhiro Iwai[10], Keiichi Namba[6,11], Masaaki Komatsu[3,4], Keiji Tanaka[7] & Masahiro Shirakawa[1]

Ubiquitin is known to be one of the most soluble and stably folded intracellular proteins, but it is often found in inclusion bodies associated with various diseases including neurodegenerative disorders and cancer. To gain insight into this contradictory behaviour, we have examined the physicochemical properties of ubiquitin and its polymeric chains that lead to aggregate formation. We find that the folding stability of ubiquitin chains unexpectedly decreases with increasing chain length, resulting in the formation of amyloid-like fibrils. Furthermore, when expressed in cells, polyubiquitin chains covalently linked to EGFP also form aggregates depending on chain length. Notably, these aggregates are selectively degraded by autophagy. We propose a novel model in which the physical and chemical instability of polyubiquitin chains drives the formation of fibrils, which then serve as an initiation signal for autophagy.

[1] Department of Molecular Engineering, Graduate School of Engineering, Kyoto University, Kyoto-Daigaku Katsura, Nishikyo-Ku, Kyoto 615-8510, Japan. [2] Graduate School of Life and Environmental Sciences, Osaka Prefecture University, Naka-ku, Sakai, Osaka 599-8531, Japan. [3] Protein Metabolism Project, Tokyo Metropolitan Institute of Medical Science, Setagaya-ku, Tokyo 156-8506, Japan. [4] Department of Biochemistry, School of Medicine, Niigata University, Chuo-ku, Niigata 951-8510, Japan. [5] Graduate School of Pharmaceutical Sciences, Kyoto University, 46-29 Yoshida-Shimoadachi, Sakyo-ku, Kyoto 606-8501, Japan. [6] Quantitative Biology Center, RIKEN, 1-3 OLABB, Osaka University 6-2-3, Furuedai, Suita, Osaka 565-0874, Japan. [7] Laboratory of Protein Metabolism, Tokyo Metropolitan Institute of Medical Science, Setagaya-ku, Tokyo 156-8506, Japan. [8] Graduate School of Medical Life Science, Yokohama City University, 1-7-29 Suehiro-cho, Tsurumi-ku, Yokohama, Kanagawa 230-0045, Japan. [9] Department of Biophysics, Graduate School of Science, Kyoto University, Oiwake-cho, Kitashirakawa, Sakyo-Ku, Kyoto 606-8502, Japan. [10] Graduate School of Medicine, Kyoto University, Yoshida-Konoe-cho, Sakyo-ku, Kyoto 606-8501, Japan. [11] Graduate School of Frontier Biosciences, Osaka University, 1-3 Yamadaoka, Suita, Osaka 565-0871, Japan. Correspondence and requests for materials should be addressed to M.S. (email: shirakawa@moleng.kyoto-u.ac.jp).

Ubiquitin is a small protein of 76 amino acids that folds into a compact globular structure. While researchers working in the field of protein chemistry widely use it as a model protein[1,2], this protein has unique physicochemical and biological properties. For example, the tertiary structure of ubiquitin is known to be one of the most rigid among eukaryotic intracellular proteins, being much more tolerant to extreme pH changes and high temperature than most cellular proteins.

Ubiquitin exerts its biological functions when it is covalently conjugated to intracellular proteins in a highly specific manner. Like phosphorylation, ubiquitylation (the modification of proteins with ubiquitin) is prevalent in both normal and pathological cellular processes[3,4] and is achieved by the successive action of ubiquitin-activating (E1), ubiquitin-conjugating (E2) and ubiquitin-ligating (E3) enzymes. Ubiquitin is first activated through the formation of an E1-ubiquitin thioester in an ATP-dependent manner and then transferred to an E2 enzyme via a thioester linkage. Finally, E3 enzymes participate in the formation of an isopeptide bond between a lysine residue on a substrate protein and the C-terminal tail of ubiquitin. This signal tag is recognized by downstream proteins containing a ubiquitin-binding domain (UBD) and can be removed from the target proteins by deubiquitinating (DUB) enzymes, which counterbalance the action of the E1–E2–E3 machinery in the cell[3].

Ubiquitin can be attached to substrates either as a single moiety (monoubiquitylation) or as several independent ubiquitin molecules (multiple monoubiquitylation). In addition, multiple ubiquitin moieties can be covalently linked via their amino (N) terminus or any of the seven lysine (K6, K11, K27, K29, K33, K48 and K63) residues on a given ubiquitin and the carboxy (C) terminus of the next ubiquitin molecule, thereby forming polymeric ubiquitin chains. These chains have mixed topology if different linkages are formed at successive positions of the chain. The most extensively characterized forms of these polymers are ubiquitin chains linked through either K48 or K63. K48-linked polyubiquitylation predominantly targets proteins for proteasomal degradation, whereas K63-linked polyubiquitylation seems to regulate protein function, subcellular localization and protein–protein interactions[3]. The roles of other types of ubiquitin chain have not been studied in great detail, but data on their specific functions are just starting to emerge, suggesting that ubiquitylation can act as a code to store and transmit information by means of specific recognition by downstream ubiquitin-binding proteins of polyubiquitin chains and/or substrate proteins[3,5].

Although exceptionally rigid and highly soluble *in vitro*, ubiquitin has been identified as a major component of protein inclusion bodies—intracellular aggregates that are associated with various intractable diseases including cancer and neurodegenerative disorders such as Alzheimer's disease, Huntington's disease and amyotrophic lateral sclerosis[6–8]. However, the formation mechanism and function of such ubiquitin-positive inclusion bodies have remained unclear ever since ubiquitin was first identified as a component of paired helical filaments in Alzheimer's disease more than 25 years ago[7]. Recently, it has been proposed that ubiquitin-positive aggregates are selectively degraded by macroautophagy (hereafter referred to as autophagy), in which isolation membranes engulf cytoplasmic constituents and the resulting autophagosomes fuse with lysosomes, leading to degradation of their constituents[9]. However, the molecular mechanism by which the aggregates are specifically degraded by autophagy is largely unknown.

Herein, we propose a novel role of ubiquitylation termed 'ubiquitin fibrils'. We show that the stability of ubiquitin is lost when ubiquitin chains are elongated, regardless of the type of ubiquitin chain. This results in the formation of polyubiquitin fibrils, which then act as a signal for clearance by autophagy.

Results

Longer ubiquitin chains have lower thermodynamic stability. We first found that the stability of ubiquitin chains significantly decreases with increasing chain length. As reported previously, monoubiquitin is highly heat stable[10]; here, differential scanning calorimetry (DSC) analysis showed that its transition temperature is 368 K. However, all polyubiquitin chains linked through Met 1 (linear), Lys 48 (K48) or Lys 63 (K63) have a transition temperature that is more than 15 K lower (Fig. 1a–c). Interestingly, longer chains show lower transition temperatures regardless of the linkage type (Fig. 1d and Supplementary Fig. 1).

In addition, while the thermal transition of monoubiquitin is reversible, those of polyubiquitin chains are irreversible, as revealed by the DSC curves observed for reheating of the heat-denatured products of ubiquitin and its polymers. Ubiquitin is soluble at and above the transition temperature (Fig. 2a), whereas polyubiquitin chains exist as insoluble small aggregates above the transition temperatures that remain insoluble even when the temperature decreases below the transition temperatures (Fig. 2b–d). These observations suggest that conjugation of ubiquitin to another ubiquitin molecule impairs its ability to refold into its native structure, and that the addition of further ubiquitin molecules leads to the transition of ubiquitin from a native state to an aggregated state at even lower temperatures.

Polyubiquitin chains form amyloid-like fibrils by heat. Unexpectedly, we found that the aggregates formed by ubiquitin chains are amyloid-like fibril assemblies. The electron microscopy (EM) images of the aggregates formed by heating linear, K48-linked and K63-linked hexaubiquitin showed that they consist of fibrils of up to 100 nm in length and ~5 nm in diameter (Fig. 3a). Similar fibrils were also formed by heating linear, K48-linked and K63-linked diubiquitin but not by heating monoubiquitin (Fig. 3a and Supplementary Fig. 2a). The morphology of these fibrils was reminiscent of amyloid-like fibrils[11]; furthermore, the polyubiquitin fibrils were all stained with Thioflavin T (ThT), the binding and fluorescence of which are considered to be indicative of amyloid-like fibrils (Fig. 3b). Circular dichroism (CD) spectra revealed that the polyubiquitin aggregates consistently displayed β-rich secondary structure, highly similar to that observed in amyloid-β (Aβ) (1–40) fibrils (Fig. 3c), supporting the idea that polyubiquitin chains form amyloid-like fibrils.

Collectively, these observations indicate that heat denaturation causes the irreversible transition of polyubiquitin chains to amyloid-like fibrils and that longer chains form fibrils at lower temperatures. For other fibrillogenic proteins, a decrease in thermodynamic stability correlates closely with a tendency towards fibril formation[12,13], which is consistent with the observed fibril formation of polyubiquitin chains.

Shear forces can induce polyubiquitin fibril formation. We also found that not only heat but also mechanical stress induces the formation of amyloid-like fibrils of polyubiquitin chains. ThT fluorescence observations indicated that polyubiquitin chains formed ThT-positive aggregates in response to moderate agitation at a rotational speed as low as 33 s^{-1}, regardless of chain length or linkage type, whereas monoubiquitin displayed no noticeable change under the same conditions (Fig. 4b and Supplementary Fig. 2b). EM images showed that the aggregates formed by

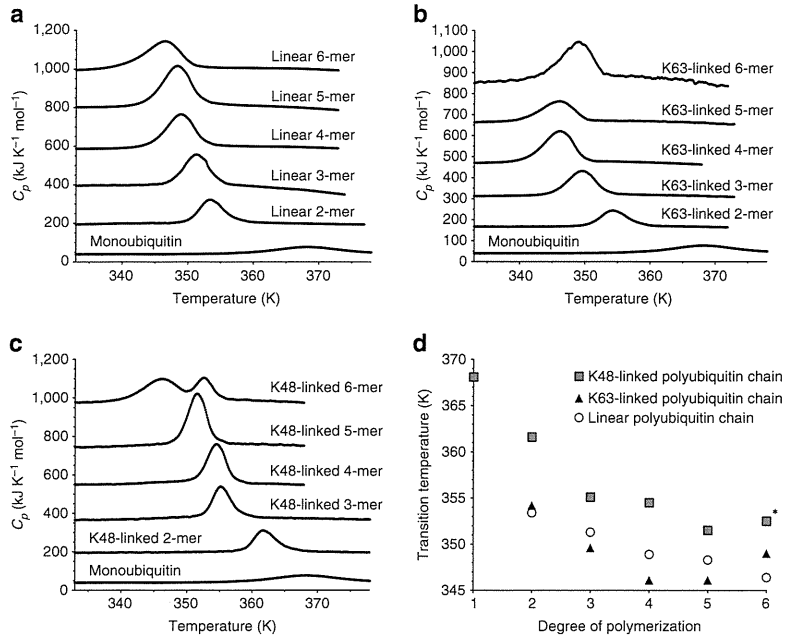

Figure 1 | Comparative analysis of the thermal denaturation for polyubiquitin chains of different length. Differential scanning calorimetry traces of monoubiquitin and linear polyubiquitin chains (**a**), K63-linked polyubiquitin chains (**b**) and K48-linked polyubiquitin chains (**c**) with up to six ubiquitin units. (**d**) Transition temperatures are plotted against chain length for K48-linked, K63-linked and linear ubiquitin chains. (*In the thermal denaturation of K48-linked hexaubiquitin, the higher transition temperature is selected.).

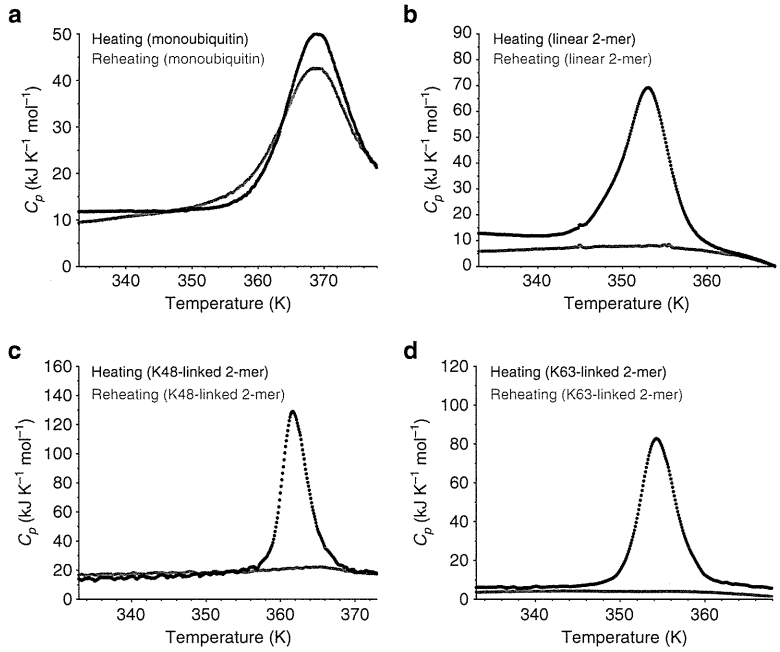

Figure 2 | Irreversible thermal unfolding of diubiquitin chains. Differential scanning calorimetry traces of monoubiquitin (**a**), linear diubiquitin (**b**), K48-linked diubiquitin (**c**) and K63-linked diubiquitin (**d**) are shown. Black traces show initial heating and red lines represent reheating. Thermal unfolding of monoubiquitin is reversible, whereas thermal unfolding of diubiquitin is irreversible.

mechanical stress are made of fibrils similar to those of amyloid-like fibrils (Fig. 4a).

Next, we measured the rate of fibril formation using a ThT fluorescence assay at a rotational speed of 25 s^{-1} to compare the influence of these hydrodynamic forces on different types of ubiquitin. The order of fibril formation tendency by shear stress was the same as that observed for the transition temperature of the polyubiquitin chains, whereby linear chains aggregated at the lowest temperature, followed by K63- and then K48-linked chains (Fig. 4c,d). Quantitative analysis using controlled shear stress in a

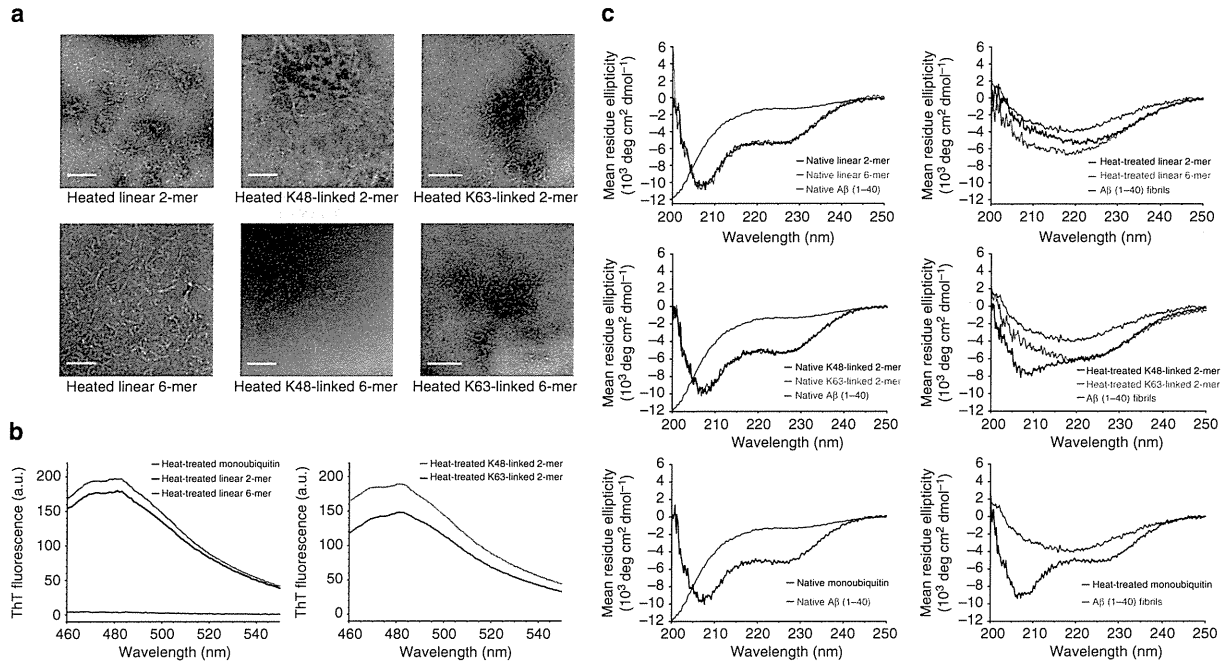

Figure 3 | Heat-treated polyubiquitin chains form amyloid-like fibrils. (**a**) Electron microscopy (EM) images of heat-treated linear diubiquitin (left upper), linear hexaubiquitin (left lower), K48-linked diubiquitin (middle upper), K48-linked hexaubiquitin (middle lower), K63-linked diubiquitin (right upper) and K63-linked hexaubiquitin (right lower). Scale bar, 100 nm. (**b**) Thioflavin T fluorescence emission spectra of heat-treated monoubiquitin (left, green), linear diubiquitin (left, black), linear hexaubiquitin (left, red), K48-linked diubiquitin (right, orange) and K63-linked diubiquitin (right, purple). (**c**) Left, circular dichroism spectra of native linear diubiquitin (upper, black), hexaubiquitin (upper, red), K48-linked diubiquitin (middle, black) and K63-linked diubiquitin (middle, red), monoubiquitin (lower, black) and Aβ (1-40) (blue). Right, circular dichroism spectra of these heat-treated samples and Aβ (1-40) fibrils (blue).

Couette cell indicated that hexaubiquitin formed fibrils in response to a shear rate of 47–60 s^{-1} (Fig. 5c), which is of the same order as that required to induce the aggregation of other fibrillogenic proteins, such as Aβ, insulin and β-lactoglobulin, in a Couette cell[14]. These results suggest that the longer the ubiquitin chains, the more easily they form fibrillar aggregates under conditions close to physiological conditions. This tendency may be caused by the increase in molecular anisotropy in polyubiquitin chains; that is, elongated molecules undergo larger anisotropic Brownian motions, and thus may be more easily affected by external mechanical stress and temperature.

Ubiquitylated proteins also form fibrils by heat or shearing. Next, we found that ubiquitylated proteins also form amyloid-like aggregates under moderate conditions. As models for substrate proteins, we chose rat calmodulin and human FK506-binding protein (FKBP12), both of which are ubiquitylated *in vivo*[15,16], and constructed their ubiquitylated forms in which monoubiquitin or linear hexaubiquitin was attached to the amino group of the N-terminal residue of the protein (that is, Ub-calmodulin, Ub_6-calmodulin, Ub-FKBP12 and Ub_6-FKBP12) (Fig. 6a). The DSC thermographs of ubiquitylated calmodulin and FKBP12 displayed irreversible thermo-transitions similar to those of ubiquitin chains, and aggregates were obtained not only by heat but also by shear stress (Fig. 6b). Although EM observations did not clearly reveal whether the aggregates contain fibrils, the CD spectra and ThT binding of the aggregates resembled to those of fibrils formed by polyubiquitin chains (Supplementary Fig. 3a,b). In contrast, non-ubiquitylated substrate proteins displayed reversible thermo-transitions and no aggregates were observed (Fig. 6b). Calmodulin conjugated to a longer polyubiquitin chain formed fibrils more easily than that conjugated to monoubiquitin (Fig. 6c, upper right). Such effect was limited in the case of FKBP12 (Fig. 6c, lower right). Taken together, these results suggest that ubiquitylation has an effect on aggregation propensity and thermal reversibility of a substrate protein and that conjugation of longer ubiquitin chains appears to enhance aggregate formation even though such effect was limited in the case of FKBP12: the effect of ubiquitin chains on fibril formation might depend on the attached substrate protein.

Autophagy specifically degraded polyubiquitin aggregates. We considered that the chain length-dependent aggregation observed *in vitro* might be related to the formation of ubiquitin-positive inclusion bodies in cells. To elucidate this possibility, we checked whether ubiquitylated proteins form aggregates intracellularly. We expressed EGFP attached to linear hexaubiquitin in which the C-terminal di-amino acids (G-G) of each ubiquitin unit were replaced by V-V ($Ub^{VV}{}_6$-EGFP) in mouse embryonic fibroblasts (MEFs). The cells displayed several EGFP-positive plaques of up to 2 μm in diameter (Fig. 7a, upper). In addition, expression of linear hexaubiquitin ($Ub^{VV}{}_6$) without any protein attached also resulted in the formation of intracellular insoluble aggregates (Supplementary Fig. 4). By contrast, in MEFs expressing monoubiquitin-attached EGFP (Ub^{VV}-EGFP), the EGFP fluorescence was smoothly distributed across the cytosol and the nucleus, as observed in control cells expressing EGFP, except for the occasional formation of a few small spots in a small fraction of cells (Fig. 7a, middle, bottom and Supplementary Fig. 4). Thus, these results indicate that whether ubiquitin chains form intracellular aggregates or not is dependent on their chain length.

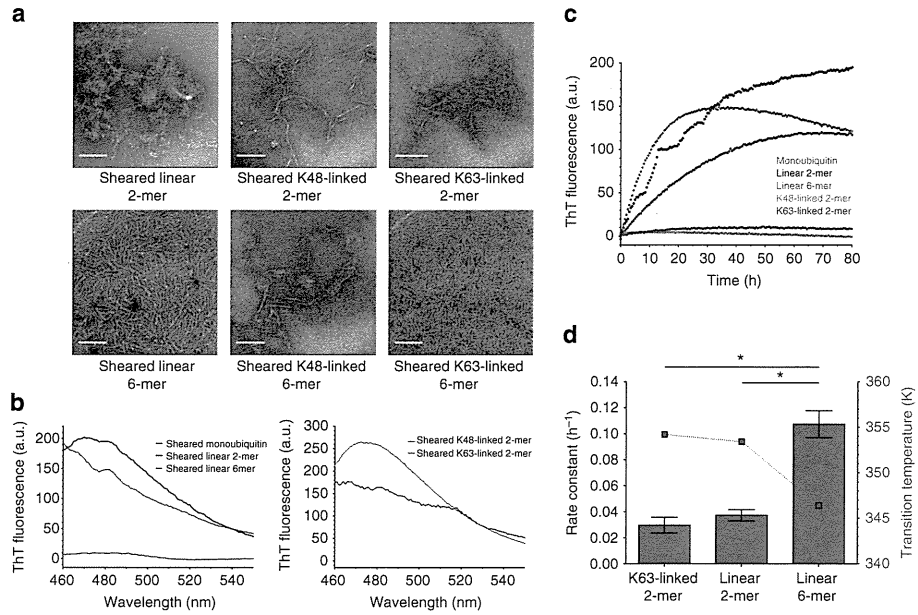

Figure 4 | Mechanical stress induces the formation of ThT-positive fibrils of polyubiquitin chains. (**a**) EM images of sheared samples: linear diubiquitin (left upper), linear hexaubiquitin (left lower), K48-linked diubiquitin (middle upper), K48-linked hexaubiquitin (middle lower), K63-linked diubiquitin (right upper) and K63-linked hexaubiquitin (right lower) show that all of these types of polyubiquitin form fibrils with amyloid-like morphology when subjected to mechanical stress. The shear stress was applied as an agitation at a rotational speed of 25 or 33 s^{-1}. Scale bar, 100 nm. (**b**) Thioflavin T fluorescence emission spectra of sheared monoubiquitin (left, green), linear diubiquitin (left, black), linear hexaubiquitin (left, red), K48-linked diubiquitin (right, orange) and K63-linked diubiquitin (right, purple). Shear stress was applied as an agitation at a rotational speed of 25 s^{-1} for 90 h. For monoubiquitin and K48-linked diubiquitin, the applied shear stress was that of 33 s^{-1} for 90 h. (**c**) Fibril formation of sheared K63-linked diubiquitin (purple), linear diubiquitin (black) and hexaubiquitin (red), as followed by ThT fluorescence. K48-linked diubiquitin (orange) and monoubiquitin (green) did not show relevant increases in fluorescence. Shear stress was applied by agitation at a rotational speed of 25 s^{-1}. (**d**) Comparative analysis of the kinetics of fibril formation by polyubiquitin chains of different linkage type and chain length with transition temperature. Rate constants were obtained by fitting the data to first-order kinetics. The values represent the average of two independent experiments. Error bars, the standard error of the mean. *$P<0.05$ (Student's t-test).

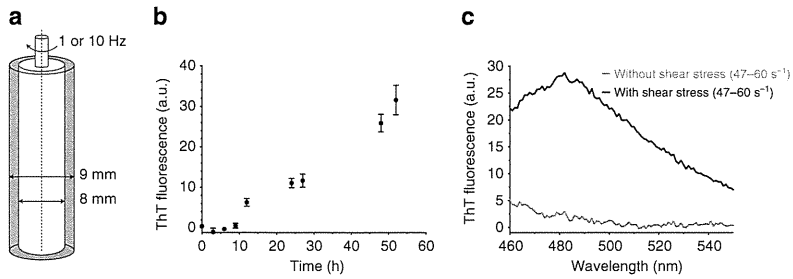

Figure 5 | Quantitative shear stress analysis in a Couette cell. (**a**) Schematic diagram of the rotational flow device used. (**b**) Fibril formation of linear hexaubiquitin in response to shear rates of 470–600 s^{-1} in a Couette cell. Error bars, the standard error of the mean. (**c**) Thioflavin T fluorescence emission spectra of non-treated linear hexaubiquitin (grey) and linear hexaubiquitin sheared in a Couette cell at a rate of 47–60 s^{-1} for 72 h (black).

Clearance of ubiquitin-positive aggregates has been shown to depend on a type of selective autophagy, which degrades aggregated proteins (aggrephagy)[9]. In aggrephagy, ubiquitin on the aggregated structures leads to the assembly of ubiquitin-adaptor proteins such as p62 and NBR1, as well as core Atg proteins. First, to determine whether p62 and NBR1 have the ability to bind to the fibrillar form of polyubiquitin or not, we used a method of solution NMR[17], in which the exchange process (binding and dissociation) is imprinted onto the transverse relaxation rates of the free UBA domain. Estimation of transverse relaxation rates (^{15}N-R_2) from heteronuclear single quantum coherence (HSQC) spectra of the respective free UBA domain and the UBA domain titrated with polyubiquitin fibrils indicated that both UBA domains interact with polyubiquitin fibrils. When the ^{15}N-labelled NBR1 domain was titrated with non-labelled polyubiquitin fibrils, its average ^{15}N-R_2 increased by $5.32 \pm 1.53\ s^{-1}$ (s.d.) in a residue-specific manner (Supplementary Fig. 5a). In the case of the UBA domain of p62, the increase was $2.94 \pm 1.10\ s^{-1}$ (s.d.) (Supplementary Fig. 5b). Indeed, it has been shown that the interaction of amyloid-β monomers with the surface of amyloid-β protofibrils leads to an increase in ^{15}N-R_2 of the monomeric form by $\sim 2\ s^{-1}$, which is of the same order as our results[18]. We thus assume that both UBA domains interact with the surface of polyubiquitin fibrils, but it will be necessary to quantitatively probe the interaction kinetics in the near future.

Finally, we tested the possibility that the Ub^{VV}_6-EGFP aggregates serve as an initiation signal for aggrephagy.

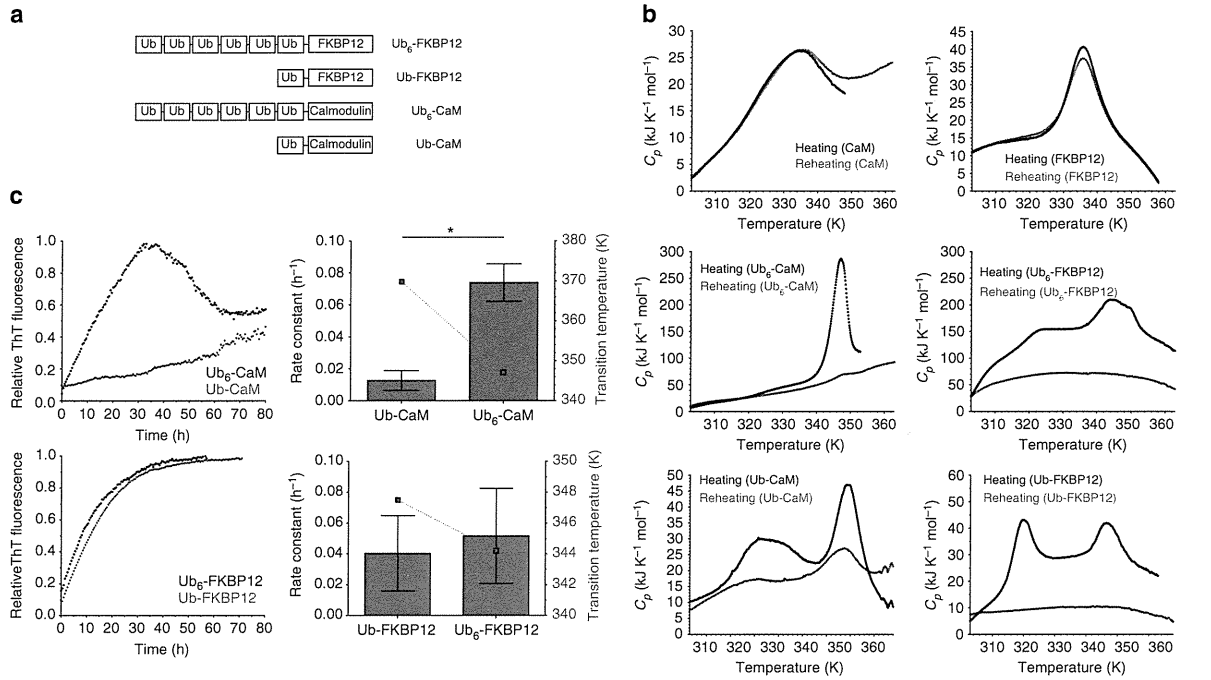

Figure 6 | Ubiquitylation impairs the folding reversibility of proteins and induces formation of amyloid-like fibrils. (**a**) Schematic diagram of ubiquitylated proteins. (**b**) Differential scanning calorimetry (DSC) traces of calmodulin (CaM) (left upper) and FKBP12 (right upper), showing that the thermal unfolding of these proteins is reversible. DSC traces of Ub_6-CaM (left middle), Ub_6-FKBP12 (right middle), Ub-CaM (left lower) and Ub-FKBP12 (right lower), indicating that the thermal unfolding of ubiquitylated proteins is irreversible. Black traces represent initial heating and red traces show reheating. (**c**) Fibril formation of sheared Ub-CaM (left upper, red), Ub_6-CaM (left upper, black), Ub-FKBP12 (left lower, red) and Ub_6-FKBP12 (left lower, black) as followed by ThT fluorescence. Comparative analysis of the fibril formation kinetics of ubiquitylated CaM (right upper) and FKBP12 (right lower) with transition temperature. Shear stress was applied as an agitation at a rotational speed of 25 s^{-1}. Rate constants were obtained by fitting the data to first-order kinetics. The values represent the average of two independent experiments. Error bars, the standard error of the mean. *$P<0.05$ (Student's *t*-test).

Autophagic flux assays revealed that expression of $Ub^{VV}{}_6$-EGFP did not affect the turnover of LC3-II, which represents autophagosome formation[19], as did expression of Ub^{VV}-EGFP (Fig. 7b). By contrast, degradation of Ser351-phosphorylated p62 in lysosomes, a hallmark of aggrephagy[20], was induced by expression of $Ub^{VV}{}_6$-EGFP, but not Ub^{VV}-EGFP (Fig. 7b). We also observed extensive co-localization of endogenous LC3 with aggregates positive for $Ub^{VV}{}_6$-EGFP (Fig. 7c). As expected[9], p62 was also recruited to these structures and found to be phosphorylated at Ser351 (Fig. 7c). The loss of autophagy-related 7 (*Atg7*), an essential gene for autophagy, inhibited degradation of $Ub^{VV}{}_6$-EGFP, p62 and Ser351-phosphorylated p62 (Fig. 7d). Expression of wild-type Atg7, but not the active site mutant Atg7 C567S (ref. 21) restored degradation of these proteins (Fig. 7e). In accordance with these biochemical data, immunofluorescence staining revealed $Ub^{VV}{}_6$-EGFP aggregate structures positive for Ser351-phosphorylated p62 in MEFs expressing the Atg7 C567S mutant (Fig. 7f). Although soluble linear-ubiquitylated proteins are partly degraded by the ubiquitin–proteasome system[22], our results indicate that aggrephagy mainly contributes to the clearance of insoluble ubiquitin-positive aggregates. In support of our data, we recently found that aggregates formed in hepatocytes with proteasome deficiency were selectively entrapped by autophagosomes, and pathological features of livers with impaired proteasome activity were exacerbated by simultaneous suppression of autophagy[23]. Remarkably, a highly sensitive polyubiquitin chain quantification method[24] revealed that insoluble proteins from livers with impaired proteasome activity contained all linkage types of polyubiquitin chains (Supplementary Fig. 6b). Likewise, we found that insoluble polyubiquitin chains accumulating in autophagy-deficient livers showed no linkage specificity[25] (Supplementary Fig. 6b). These *in vivo* analyses suggest that all types of polyubiquitin chains on proteins have the potential to induce their fibrillar aggregate formation followed by induction of autophagy, which serves a cytoprotective function.

Discussion

In this manuscript, we describe a novel and unexpected nature of ubiquitin; that is, in contrast to the rigid structure of a single ubiquitin, ubiquitin becomes thermodynamically unstable when it is conjugated to another ubiquitin molecule or to another protein. This is unexpected because proteins with repeating identical domains have been considered to show increasing folding stability with an increasing number of domains[26].

So why does length-dependent destabilization occur in polyubiquitin chains? One possibility is domain swapping, in which a secondary or tertiary element of a monomeric protein is replaced by the corresponding element of another protein molecule[27]. Recently, it has been reported that connecting of immunoglobulin domains in tandem causes fibril formation via a domain-swapping mechanism[28,29]. Intriguingly, a similar domain-swapping event has been proposed for diubiquitin[30]. Therefore, elongation of ubiquitin into a ubiquitin chain may promote the formation of both intra- and inter-molecular domain-swapped structures. This may explain the length-dependent thermodynamic destabilization that we observed in polyubiquitin chains.

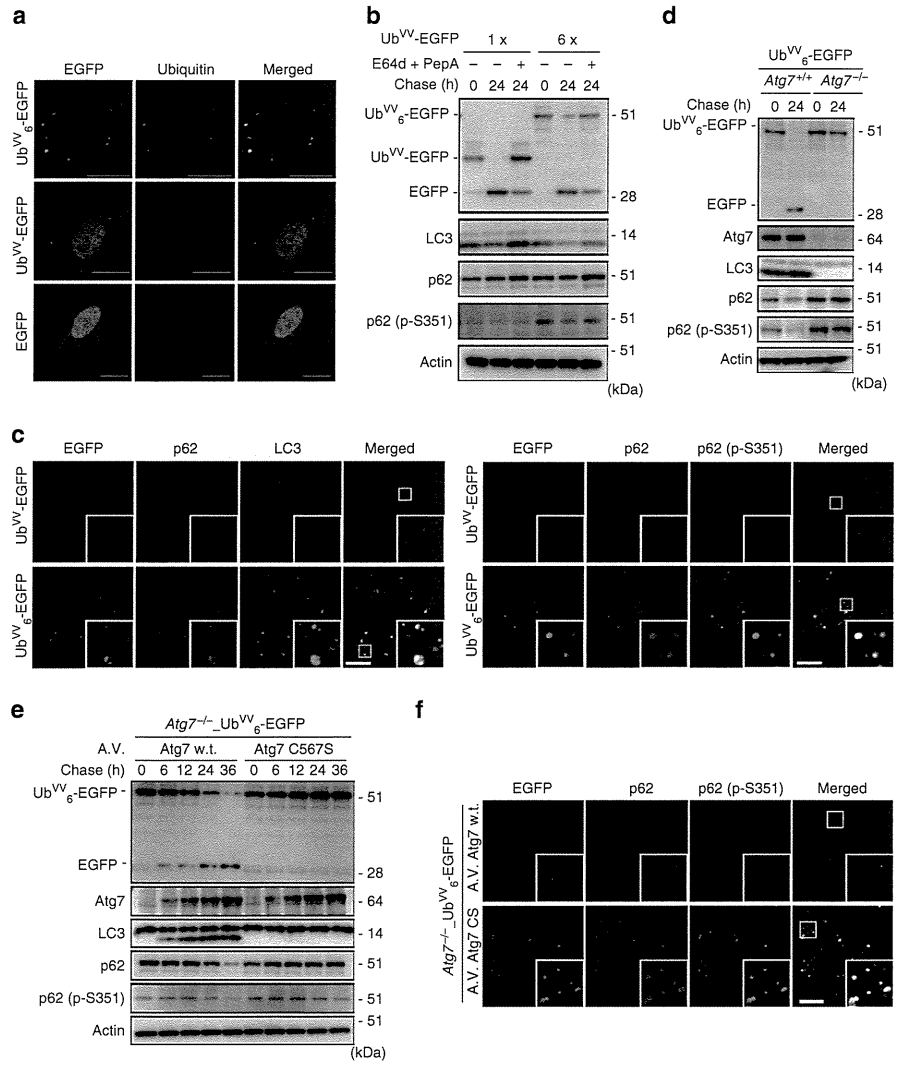

Figure 7 | *In vivo* aggregation of polyubiquitin chains and degradation by macroautophagy. (**a**) MEFs were transiently transfected with $Ub^{VV}{}_6$-EGFP (top), Ub^{VV}-EGFP (middle) or EGFP (bottom) and imaged 48 h after transfection. No ubiquitin-positive aggregates were detected in cells expressing Ub^{VV}-EGFP and EGFP, whereas ubiquitin-positive aggregates of up to 2 μm in diameter were observed in cells expressing $Ub^{VV}{}_6$-EGFP. Scale bar, 20 μm. Data are representative of three independent experiments. (**b**) Immortalized wild-type MEFs harbouring two regulator gene cassettes, CAG-rtTA and either TRE-$Ub^{VV}{}_6$-EGFP or TRE-Ub^{VV}-EGFP, were cultured for 24 h in the presence of Dox to induce expression of $Ub^{VV}{}_6$-EGFP or Ub^{VV}-EGFP. Subsequently, the cells were cultured in the absence of Dox for 24 h. E64d and pepstatin were added as indicated. The cell lysates were prepared and immunoblotted with the indicated antibodies. Data are representative of two independent experiments. (**c**) The MEFs shown in **b** were cultured for 24 h in the presence of Dox to induce expression of $Ub^{VV}{}_6$-EGFP or Ub^{VV}-EGFP, and then immunostained with p62 and LC3 antibodies or p62 and Ser351-phosphorylated p62 antibodies. Scale bar, 20 μm. Data are representative of three independent experiments. (**d**) Immortalized wild-type and *Atg7*-deficient MEFs were stably transfected with two regulator gene cassettes, CAG-rtTA and TRE-$Ub^{VV}{}_6$-EGFP. The cells were cultured for 24 h in the presence of Dox to induce expression of $Ub^{VV}{}_6$-EGFP. Subsequently, the cells were cultured in the absence of Dox for 24 h. The cell lysates were prepared and immunoblotted with the indicated antibodies. Data are representative of two independent experiments. (**e**) After induction of $Ub^{VV}{}_6$-EGFP in the *Atg7*-knockout MEFs as shown in **d**, Atg7 or Atg7 C567S was expressed using an adenovirus system. At the indicated time points, cell lysates were prepared and immunoblotted with the indicated antibodies. Data are representative of two independent experiments. (**f**) MEFs treated as shown in **e** were immunostained with p62 and Ser351-phosphorylated p62 antibodies, 36 h after infection with the indicated adenovirus vectors. Scale bar, 20 μm. Data are representative of three independent experiments. A.V., adenovirus; w.t., wild type.

The thermodynamic stability of monoubiquitin is exceptionally high. Even polyubiquitin chains may have a higher thermodynamic stability than other cytosolic proteins. However, the temperature at which long polyubiquitin chains form fibrils is comparable with that at which several other amyloid-prone proteins form fibrils: myoglobin (horse skeletal muscle) forms fibrils by heating to 338 K (ref. 31) and β-lactoglobulin does so by heating to 353 K (ref. 32). In addition, it is noteworthy that long polyubiquitin chains form insoluble fibrils at moderate shear stress under physiological temperature and pH (Fig. 5b,c), implying that ubiquitin fibrils may form under physiological conditions even though the experimental conditions did not exactly mimic *in vivo* situations. It is currently not well understood, in what capacity melting temperatures of proteins

determined *in vitro* correlate with protein aggregation *in vivo*. As the intracellular environment markedly differs from the test tube system in which we determined these unfolding temperatures, it is plausible that additional factors trigger the aggregation of a given ubiquitin chain in living cells.

An involvement of ubiquitylation in the sequestration and degradation of misfolded proteins has been already described[33,34] and it is reported that monoubiquitylation triggers sequestration of α-synuclein aggregates[35]. However, the mechanism of how ubiquitylation induces aggregation-associated sequestration has remained elusive. Our *in vitro* data suggest that ubiquitylation has an effect on aggregation propensity and thermal folding reversibility of a substrate protein (Fig. 6b), which could be connected to the sequestration and degradation of misfolded proteins by ubiquitylation. But, how monoubiquitylation causes protein aggregation and why the kinetics of fibril formation depends on a substrate protein have been elusive; therefore, further analysis is needed to clarify these critical issues. In addition, our *in vivo* data indicate that simple overexpression of EGFP attached to linear hexaubiquitin, but not monoubiquitin, was sufficient for the formation of aggregate structures in cells (Fig. 7a). This observation underscores that fibril formation occurs *in vivo*, when polyubiquitylated proteins, which accumulate owing to proteasome dysfunction or dysregulated deubiquitylation, are exposed to intracellular forces arising from cytoplasmic streaming, macromolecular crowding or (non-) specific protein interactions over a period of time. It will be necessary to determine the kind of intracellular forces involved and the length of time needed for ubiquitin fibril formation.

Although autophagy has been considered to be a non-selective bulk degradation system of the cell, mounting evidence is pointing to other autophagy modes that selectively degrade aggregated proteins (aggrephagy), damaged mitochondria (mitophagy) and invading bacterial cells (xenophagy)[36]. Thus, inactivation of autophagy leads to an accumulation of both cytoplasmic protein inclusions and excess deformed organelles, which causes liver injury, diabetes, heart disease and neurodegeneration[37]. Under the conditions of each processes, namely aggrephagy, mitophagy and xenophagy, different target proteins are ubiquitylated by distinct E3s such as Chip, Parkin and LRSAM1 (ref. 36), implying that polyubiquitin chains of varying topology give rise to different types of selective autophagy. Nevertheless, in any of these types of selective autophagy, ubiquitylation triggers a common transduction signal—namely, the assembly of core Atg proteins and adaptor proteins such as p62 around the autophagic cargo. Therefore, our observation that the formation of fibrils by polyubiquitin chains was linkage-type independent (Fig. 1d) suggests that the ubiquitin fibril plays a critical role in selective autophagy. We propose that polyubiquitin chains have two distinct biological roles: one is a linkage-specific signal for proteasome-mediated degradation and other non-proteolytic pathways. The other role is a linkage-independent, but length-dependent inducer of fibrillar structures for selective clearance by autophagy. The latter pathway would be cytoprotective: such insolubilization would prevent any undesired activities of the substrate proteins before protein aggregates start to accumulate in cells[38,39].

In healthy cells, protein aggregates sequestered by ubiquitylation are degraded by selective autophagy before they form large inclusions (Fig. 7b). On the other hand, the activity of the ubiquitin–proteasome system decreases with aging[40] and loss (that is, dysfunction or inactivation) of autophagy has been previously described in senescent cells[41,42]. Accordingly, most elderly patients suffering from neurodegenerative diseases may have insufficient activity of autophagy—namely the capacity to specifically degrade intracellular ubiquitin-positive aggregates (ubiquitin fibrils). As a result, aging- and/or disease-associated inactivation of the proteasome and/or autophagy pathways may result in cytotoxic accumulation of ubiquitin-positive aggregates, even in the absence of aggregate-prone proteins related to conformational diseases. Ultimately, such ubiquitin-positive aggregates may be sequestered into so-called inclusion bodies, particularly in non-dividing cells such as neurons and myocytes. We propose that this is why most inclusion bodies observed in neurodegenerative diseases that have been reported contain ubiquitin as a major constituent[7]. A unique feature of polyubiquitin chains is that it is the wild-type protein that forms fibrils; this feature is in stark contrast to other amyloid-forming proteins, many of which are truncated or carry mutations such as Aβ or SOD1 (refs 12,43). Therefore, our proposed model would take into account the pathological hallmarks of human sporadic proteinopathies without genetic mutations.

Collectively, intracellular ubiquitylation not only aids recruitment of proteins to the proteasome in solution, but also shields the cell from undesired activities of substrate proteins by encapsulating them in solid aggregates. Last, the structure of the ubiquitin fibrils acts as an initiation signal for autophagy. To our knowledge, this paper is the first to report that ubiquitin chains function as a driving force to form fibrillar aggregates that have chain-length dependency but no linkage specificity and that these aggregates, whose accumulation disturbs cellular homeostasis, can act as direct substrates for removal by selective autophagy. The two biological roles of polyubiquitin chains (that is, a canonical linkage-specific signal and an inducer of fibril formation) may function independently and, accordingly, future studies should aim to elucidate the underlying mechanism that discriminates between them in a spatiotemporal fashion.

Methods

Protein preparation. Mouse E1 enzyme UBA1 was expressed in Sf9 cells, yeast K63-linked E2 enzyme Ubc13-Mms2 complex was expressed in *Escherichia coli* strain BL21 Codon plus (*DE3*) RIL and all other recombinant proteins were expressed in *E. coli* strain BL21 (*DE3*). Untagged human ubiquitin was purified by ion exchange and size-exclusion chromatography[44]. Human 12-kDa FK506-binding protein (FKBP12) was expressed as a fusion protein with an N-terminal glutathione *S*-transferase (GST) and small ubiquitin-like modifier (SUMO)-1 protein tag. After cleavage of the protein tag by GST-SENP2 protease, FKBP12 was further purified by ion exchange and size-exclusion chromatography[45]. Untagged rat calmodulin was purified by Phenyl Sepharose Fast Flow (GE Healthcare) and size-exclusion chromatography[46]. N-terminal hexa-histidine (His_6) tagged mouse UBA1, K48-linked E2 enzyme E2-25K and linear E2 enzyme UbcH7 was purified by Ni-NTA affinity chromatography[22,44,47]. Yeast Ubc13 was co-expressed with N-terminal His_6-tagged yeast Mms2, followed by purification by Ni-NTA affinity and size-exclusion chromatography[44]. Human HOIL-1L (1–191) was co-expressed with N-terminal His_6-tagged human HOIP (476–1,072) and the HOIL-1L-HOIP complex (human linear E3 ligase) was purified by Ni-NTA affinity chromatography[22]. K48-linked and K63-linked polyubiquitin chains were enzymatically synthesized by the appropriate E1, E2 and E3 enzymes shown above[47]. Linear polyubiquitin chains were both expressed recombinantly and synthesized enzymatically[22,47]. Separation of cyclic and non-cyclic K48-linked polyubiquitin chains has not been performed. Met1-monoubiquitylated and hexaubiquitylated FKBP12, which contain an additional DGGS sequence between ubiquitin and FKBP12, and an HRV3C-cleavable C-terminal His_6-tag, were expressed and purified by Ni-NTA affinity chromatography. After cleavage of the C-terminal His_6-tag by HRV3C protease, the fusion proteins were further purified by ion exchange and size-exclusion chromatography. Met1-mono- and hexaubiquitylated calmodulin containing an HRV3C-cleavable C-terminal His_6-tag were expressed and purified in the same manner. Calcium ions, to which calmodulin and ubiquitylated calmodulin bind with high affinity, were removed by EGTA during the purification.

Differential scanning calorimetry. Thermal denaturation curves were acquired by a Nano DSC instrument (TA Instruments Inc.). The scan rate was 1 K min^{-1}, and protein concentrations ranged from 0.2 to 1 mg ml^{-1}. The buffer used in the calorimetric experiments of (poly-)ubiquitin and (Met1-ubiquitylated-)calmodulin was phosphate-buffered saline (PBS; 137 mM NaCl, 8.1 mM Na_2HPO_4, 2.68 mM KCl, 1.47 mM KH_2PO_4, pH 7.4). In the case of (Met1-ubiquitylated-)FKBP12, 0.5 mM TCEP was included to prevent cysteine-mediated dimerization. Reheating experiments were performed in the same manner after heating until the peak

finished and mild cooling to room temperature. Analysis was performed using CpCalc (TA Instruments Inc.) and data were reported as heat capacity (kJ K^{-1} mol^{-1}). The transition temperature was defined as the temperature corresponding to the peak top. However, precise thermodynamic parameters could not be acquired owing to the irreversibility of the melting reaction *in vitro*.

Transmission electron microscopy. TEM images were obtained using a JEM-1011 transmission electron microscope (JEOL). All the samples were diluted to 100 μg ml^{-1} in 25 mM Tris-HCl pH 8 and 150 mM NaCl, loaded onto a carbon grid and negatively stained with 2% (w/v) uranyl acetate or PTA (phosphotungstic acid). Scale bars were estimated by measuring tobacco mosaic virus under identical conditions. Images were analysed via ImageJ 1.45s.

Fluorescence spectroscopy. Fluorescence was quantified on a FluoroMax4 (HORIBA) spectrometer at 298 K by excitation at 440 nm with acquisition of emission spectra over wavelengths of 460 to 550 nm with the slit width set at 5 nm. Monomeric samples were diluted to a final concentration of 5.8 μM in analysis buffer containing 25 mM Tris-HCl pH 8, 150 mM NaCl and 25 μM thioflavin T. Polyubiquitin chains and ubiquitylated proteins were diluted to an equimolar concentration (5.8 μM) of monomeric ubiquitin subunits. In the case of (Met1-ubiquitylated-)FKBP12, 0.5 mM TCEP was included. The spectral contribution of the buffer was subtracted from the acquired spectra. To monitor fibril growth, the ThT fluorescence intensity at 480 nm was measured every 30 min with continuous stirring at 25 s^{-1} by a stirrer bar (Bel-Art Products). The fluorescence intensities at time t after the start, $I(t)$, were fitted to the equation $I(t) = I(t_\infty)$ $[1 - \exp(-kt)]$ to obtain the rate constant k.

Circular dichroism spectroscopy. Circular dichroism spectra were collected on a J-820 spectrophotometer (JASCO) from 250 to 200 nm in 0.1-nm intervals. Data were measured at 298 K with a 1-mm path length in 25 mM Tris-HCl pH 8, 150 mM NaCl, containing 0.5 mM TCEP in the case of (Met1-ubiquitylated-) FKBP12. The concentration of all proteins used in the measurements was adjusted to 0.2 mg ml^{-1}. Data were reported as mean residue ellipticities. The spectral contributions by the buffer were subtracted.

Shear stress in a Couette cell. Controlled shear stress[48] was produced by an SM-101 instrument (As One), which incorporated an iron inner cylinder (8 mm) in a custom-built quartz cell (9 mm) at room temperature (298 K; Fig. 5a). Samples treated with shear stress were collected from the shear cell at each time point. Linear hexaubiquitin was diluted to an equimolar concentration (116 μM) of monomeric ubiquitin subunits in analysis buffer containing 25 mM Tris-HCl pH 8 and 150 mM NaCl. The samples were exposed to a moderate shear rate of 47–60 or 470–600 s^{-1}. The shear rate in the Couette cell is calculated as $\dot{\gamma}(r) = \frac{2\Omega}{r^2\left(R_i^{-2} - R_0^{-2}\right)}$, where Ω is the angular frequency of the rotor (rad s^{-1}), R_i is the radius of the rotor and R_0 represents the radius of the quartz cell[49,50].

Transfection. MEFs were maintained in DMEM (Gibco) with 10% fetal bovine serum, penicillin (100 U ml^{-1}) and streptomycin (100 μg ml^{-1}). The cells were detached from the dish with 0.025% trypsin, and 2×10^6 cells were centrifuged at 100 *g* for 10 min. The cell pellet was gently suspended in 100 μl of MEF Nucleofector solution (Amaxa) with 10 μg of expression plasmid pcDNA 3.1 cloned with EGFP, Ub^{VV}-EGFP or $Ub^{VV}{}_6$-EGFP, which contain an additional MASH sequence in front of ubiquitin and an additional GGSG sequence between ubiquitin and EGFP. Ub^{VV} indicates a C-terminal Val-Val ubiquitin mutant with the sequence MQIFVKTLTGKTITLEVESSDTIDNVKAKIQDKEGIPPDQQRLIFAGKQLEDGR TLADYNIQKESTLHLVLRLRVV. The cell suspension was electroporated by using the T-020 program (Amaxa).

Immunoblot analysis. Samples were separated using 12% NuPAGE Bis-Tris gels (Invitrogen) in MOPS-SDS buffer, followed by transferring to polyvinylidene difluoride membranes. Antibodies against ubiquitin (Santa Cruz Biotechnology, Inc., P4D1), p62 (Progen Biotechnik, GP62-C), LC3B (Cell Signaling Technology, #2775), GFP (Invitrogen) and Actin (Chemicon International, Inc., MAB1501R) were purchased from the indicated suppliers. Anti-phosphorylated p62 polyclonal antibody was raised in rabbits using the peptide Cys + KEVDP(pS)TGELQSL as an antigen[20]. The polyclonal antibody against Atg7 was raised in rabbits using the synthetic peptide VVAPGDSTRDRTLDQQ, which corresponds to the amino acid residues 556–571 as an antigen[21]. For blotting, indicated antibodies were used at a dilution of 1:500. Uncropped blots are shown in Supplementary Fig. 8.

Immunocytochemistry. Cells grown on coverslips were fixed with 4% paraformaldehyde in PBS and permeabilized with 0.1% Triton X-100 or 50 μg ml^{-1} digitonin in PBS. After washing with PBS, the coverslips were blocked with PBS containing 10% normal goat serum (Jackson Immuno Research) for 1 h or 0.1% (w/v) gelatin (Sigma-Aldrich) in PBS for 30 min, and then incubated overnight with 150 or 200-fold diluted solution of primary antibodies against ubiquitin (Dako, Z 0458), p62 (Progen Biotechnik, GP62-C), Ser351-phosphorylated p62 and/or LC3B (Cell Signaling Technology, #2775). After washing with PBS, the coverslips were incubated with a 1,000-fold diluted solution of Alexa Fluor-conjugated goat anti-guinea pig and/or anti-rabbit IgG secondary antibodies (Invitrogen) for 1 h. Images were taken by confocal laser scanning microscopy using an FV1000 microscope (Olympus). Z-projection stack images were acquired with z-steps of 0.5 μm. Image contrast and brightness were adjusted using Photoshop CS4 (Adobe Systems, Inc.).

References

1. Ibarra-Molero, B., Loladze, V. V., Makhatadze, G. I. & Sanchez-Ruiz, J. M. Thermal versus guanidine-induced unfolding of ubiquitin. An analysis in terms of the contributions from charge-charge interactions to protein stability. *Biochemistry* **38,** 8138–8149 (1999).
2. Lindorff-Larsen, K., Best, R. B., Depristo, M. A., Dobson, C. M. & Vendruscolo, M. Simultaneous determination of protein structure and dynamics. *Nature* **433,** 128–132 (2005).
3. Komander, D. & Rape, M. The ubiquitin code. *Annu Rev Biochem.* **81,** 203–229 (2012).
4. Weissman, A. M. Themes and variations on ubiquitylation. *Nat. Rev. Mol. Cell Biol.* **2,** 169–178 (2001).
5. Dikic, I., Wakatsuki, S. & Walters, K. J. Ubiquitin-binding domains—from structures to functions. *Nat. Rev. Mol. Cell Biol.* **10,** 659–671 (2009).
6. Gallo, J. M. & Anderton, B. H. Brain diseases. Ubiquitous variations in nerves. *Nature* **337,** 687–688 (1989).
7. Mori, H., Kondo, J. & Ihara, Y. Ubiquitin is a component of paired helical filaments in Alzheimer's disease. *Science* **235,** 1641–1644 (1987).
8. Ross, C. A. & Poirier, M. A. Protein aggregation and neurodegenerative disease. *Nat. Med.* **10**(Suppl): S10–S17 (2004).
9. Kirkin, V., McEwan, D. G., Novak, I. & Dikic, I. A role for ubiquitin in selective autophagy. *Mol. Cell* **34,** 259–269 (2009).
10. Wintrode, P. L., Makhatadze, G. I. & Privalov, P. L. Thermodynamics of ubiquitin unfolding. *Proteins* **18,** 246–253 (1994).
11. Olzscha, H. *et al.* Amyloid-like aggregates sequester numerous metastable proteins with essential cellular functions. *Cell* **144,** 67–78 (2011).
12. Chiti, F., Stefani, M., Taddei, N., Ramponi, G. & Dobson, C. M. Rationalization of the effects of mutations on peptide and protein aggregation rates. *Nature* **424,** 805–808 (2003).
13. Vassall, K. A. *et al.* Decreased stability and increased formation of soluble aggregates by immature superoxide dismutase do not account for disease severity in ALS. *Proc. Natl Acad. Sci. USA* **108,** 2210–2215 (2011).
14. Bekard, I. B., Asimakis, P., Bertolini, J. & Dunstan, D. E. The effects of shear flow on protein structure and function. *Biopolymers* **95,** 733–745 (2011).
15. Laub, M. *et al.* Modulation of calmodulin function by ubiquitin-calmodulin ligase and identification of the responsible ubiquitylation site in vertebrate calmodulin. *Eur. J. Biochem.* **255,** 422–431 (1998).
16. Wagner, S. A. *et al.* A proteome-wide, quantitative survey of *in vivo* ubiquitylation sites reveals widespread regulatory roles. *Mol. Cell. Proteomics* **10,** M111.013284 (2011).
17. Fawzi, N. L., Ying, J., Torchia, D. A. & Clore, G. M. Probing exchange kinetics and atomic resolution dynamics in high-molecular-weight complexes using dark-state exchange saturation transfer NMR spectroscopy. *Nat. Protoc.* **7,** 1523–1533 (2012).
18. Fawzi, N. L., Ying, J., Ghirlando, R., Torchia, D. A. & Clore, G. M. Atomic-resolution dynamics on the surface of amyloid-β protofibrils probed by solution NMR. *Nature* **480,** 268–272 (2011).
19. Kabeya, Y. *et al.* LC3, a mammalian homologue of yeast Apg8p, is localized in autophagosome membranes after processing. *EMBO J.* **19,** 5720–5728 (2000).
20. Ichimura, Y. *et al.* Phosphorylation of p62 activates the Keap1-Nrf2 pathway during selective autophagy. *Mol. Cell* **51,** 618–631 (2013).
21. Tanida, I. *et al.* Apg7p/Cvt2p: a novel protein-activating enzyme essential for autophagy. *Mol. Biol. Cell* **10,** 1367–1379 (1999).
22. Kirisako, T. *et al.* A ubiquitin ligase complex assembles linear polyubiquitin chains. *EMBO J.* **25,** 4877–4887 (2006).
23. Kageyama, S. *et al.* Proteasome dysfunction activates autophagy and the Keap1-Nrf2 pathway. *J. Biol. Chem.* **289,** 24944–24955 (2014).
24. Tsuchiya, H., Tanaka, K. & Saeki, Y. The parallel reaction monitoring method contributes to a highly sensitive polyubiquitin chain quantification. *Biochem. Biophys. Res. Commun.* **436,** 223–229 (2013).
25. Riley, B. E. *et al.* Ubiquitin accumulation in autophagy-deficient mice is dependent on the Nrf2-mediated stress response pathway: a potential role for protein aggregation in autophagic substrate selection. *J. Cell Biol.* **191,** 537–552 (2010).
26. Cortajarena, A. L. & Regan, L. Calorimetric study of a series of designed repeat proteins: modular structure and modular folding. *Protein Sci.* **20,** 336–340 (2011).
27. Bennett, M. J., Sawaya, M. R. & Eisenberg, D. Deposition diseases and 3D domain swapping. *Structure* **14,** 811–824 (2006).

28. Borgia, M. B. *et al.* Single-molecule fluorescence reveals sequence-specific misfolding in multidomain proteins. *Nature* **474,** 662–665 (2011).
29. Wright, C. F., Teichmann, S. A., Clarke, J. & Dobson, C. M. The importance of sequence diversity in the aggregation and evolution of proteins. *Nature* **438,** 878–881 (2005).
30. Xia, F., Thirumalai, D. & Gräter, F. Minimum energy compact structures in force-quench polyubiquitin folding are domain swapped. *Proc. Natl Acad. Sci. USA* **108,** 6963–6968 (2011).
31. Fändrich, M. *et al.* Myoglobin forms amyloid fibrils by association of unfolded polypeptide segments. *Proc. Natl Acad. Sci. USA* **100,** 15463–15468 (2003).
32. Arnaudov, L. N., de Vries, R., Ippel, H. & van Mierlo, C. P. Multiple steps during the formation of beta-lactoglobulin fibrils. *Biomacromolecules* **4,** 1614–1622 (2003).
33. Kaganovich, D., Kopito, R. & Frydman, J. Misfolded proteins partition between two distinct quality control compartments. *Nature* **454,** 1088–1095 (2008).
34. Shiber, A., Breuer, W., Brandeis, M. & Ravid, T. Ubiquitin conjugation triggers misfolded protein sequestration into quality control foci when Hsp70 chaperone levels are limiting. *Mol. Biol. Cell* **24,** 2076–2087 (2013).
35. Rott, R. *et al.* Monoubiquitylation of alpha-synuclein by seven in absentia homolog (SIAH) promotes its aggregation in dopaminergic cells. *J. Biol. Chem.* **283,** 3316–3328 (2008).
36. Johansen, T. & Lamark, T. Selective autophagy mediated by autophagic adapter proteins. *Autophagy* **7,** 279–296 (2011).
37. Mizushima, N., Levine, B., Cuervo, A. M. & Klionsky, D. J. Autophagy fights disease through cellular self-digestion. *Nature* **451,** 1069–1075 (2008).
38. Bjørkøy, G. *et al.* p62/SQSTM1 forms protein aggregates degraded by autophagy and has a protective effect on huntingtin-induced cell death. *J. Cell Biol.* **171,** 603–614 (2005).
39. Zhou, X. *et al.* Rheb controls misfolded protein metabolism by inhibiting aggresome formation and autophagy. *Proc. Natl Acad. Sci. USA* **106,** 8923–8928 (2009).
40. Carrard, G., Bulteau, A. L., Petropoulos, I. & Friguet, B. Impairment of proteasome structure and function in aging. *Int. J. Biochem. Cell Biol.* **34,** 1461–1474 (2002).
41. Cuervo, A. M. *et al.* Autophagy and aging: the importance of maintaining "clean" cells. *Autophagy* **1,** 131–140 (2005).
42. Rubinsztein, D. C., Mariño, G. & Kroemer, G. Autophagy and aging. *Cell* **146,** 682–695 (2011).
43. Chiti, F. & Dobson, C. M. Amyloid formation by globular proteins under native conditions. *Nat. Chem. Biol.* **5,** 15–22 (2009).
44. Tenno, T. *et al.* Structural basis for distinct roles of Lys63- and Lys48-linked polyubiquitin chains. *Genes Cells* **9,** 865–875 (2004).
45. Tsukiji, S., Miyagawa, M., Takaoka, Y., Tamura, T. & Hamachi, I. Ligand-directed tosyl chemistry for protein labeling *in vivo*. *Nat. Chem. Biol.* **5,** 341–343 (2009).
46. Hayashi, N., Matsubara, M., Takasaki, A., Titani, K. & Taniguchi, H. An expression system of rat calmodulin using T7 phage promoter in *Escherichia coli*. *Protein Expr. Purif.* **12,** 25–28 (1998).
47. Morimoto, D. *et al.* Purification, crystallization and preliminary crystallographic studies of Lys48-linked polyubiquitin chains. *Acta Crystallogr. Sect. F Struct. Biol. Cryst. Commun.* **66,** 834–837 (2010).
48. Hill, E. K., Krebs, B., Goodall, D. G., Howlett, G. J. & Dunstan, D. E. Shear flow induces amyloid fibril formation. *Biomacromolecules* **7,** 10–13 (2006).
49. Macosko, C. W. *Rheology: Principles, Measurements, and Applications* (Wiley-VCH, 1994).
50. Ohgo, K., Bagusat, F., Asakura, T. & Scheler, U. Investigation of structural transition of regenerated silk fibroin aqueous solution by Rheo-NMR Spectroscopy. *J. Am. Chem. Soc.* **130,** 4182–4186 (2008).

Acknowledgements

We thank I. Hamachi and K. Matsuda for circular dichroism spectroscopy, S. Kiyonaka and Y. Mori for transfection and immunofluorescence staining, DKSH Japan Limited for preliminary differential scanning calorimetry and H. Watanabe for discussions. This work was supported by research fellowships from the Japan Society for the Promotion of Science for Young Scientists (J.S.P.S.).

Author contributions

D.M. and M.S. designed the experiments. D.M. and E.W. conducted most experiments. H.F. performed DSC analysis. M.H. assisted with fluorescence and CD spectroscopy. T.F. and K.N. contributed to electron microscopy experiments. Y.-S.S. and S.K performed the cell biological studies. H.T. and Y.S. performed mass spectroscopic analysis. K.A., M.A., H.T. and K.I. supervised the project. M.K. and K.T. coordinated the research. D.M., E.W., K.T., M.K. and M.S. wrote the manuscript. All the authors discussed the results and commented on the manuscript.

Additional information

Supplementary Information accompanies this paper at http://www.nature.com/naturecommunications

Competing financial interests: The authors declare no competing financial interests.

Reprints and permission information is available online at http://npg.nature.com/reprintsandpermissions/

How to cite this article: Morimoto, D. *et al.* The unexpected role of polyubiquitin chains in the formation of fibrillar aggregates. *Nat. Commun.* 6:6116 doi: 10.1038/ncomms7116 (2015).

LETTER

doi:10.1038/nature13392

Ubiquitin is phosphorylated by PINK1 to activate parkin

Fumika Koyano[1,2], Kei Okatsu[1,2], Hidetaka Kosako[3], Yasushi Tamura[4], Etsu Go[1], Mayumi Kimura[1], Yoko Kimura[1,5], Hikaru Tsuchiya[1], Hidehito Yoshihara[1], Takatsugu Hirokawa[6], Toshiya Endo[7,8], Edward A. Fon[9], Jean-François Trempe[10], Yasushi Saeki[1], Keiji Tanaka[1] & Noriyuki Matsuda[1,11]

PINK1 **(PTEN induced putative kinase 1) and** ***PARKIN*** **(also known as** ***PARK2*****) have been identified as the causal genes responsible for hereditary recessive early-onset Parkinsonism[1,2]. PINK1 is a Ser/Thr kinase that specifically accumulates on depolarized mitochondria, whereas parkin is an E3 ubiquitin ligase that catalyses ubiquitin transfer to mitochondrial substrates[3–5]. PINK1 acts as an upstream factor for parkin[6,7] and is essential both for the activation of latent E3 parkin activity[8] and for recruiting parkin onto depolarized mitochondria[8–12]. Recently, mechanistic insights into mitochondrial quality control mediated by PINK1 and parkin have been revealed[3–5], and PINK1-dependent phosphorylation of parkin has been reported[13–15]. However, the requirement of PINK1 for parkin activation was not bypassed by phosphomimetic parkin mutation[15], and how PINK1 accelerates the E3 activity of parkin on damaged mitochondria is still obscure. Here we report that ubiquitin is the genuine substrate of PINK1. PINK1 phosphorylated ubiquitin at Ser 65 both** ***in vitro*** **and in cells, and a Ser 65 phosphopeptide derived from endogenous ubiquitin was only detected in cells in the presence of PINK1 and following a decrease in mitochondrial membrane potential. Unexpectedly, phosphomimetic ubiquitin bypassed PINK1-dependent activation of a phosphomimetic parkin mutant in cells. Furthermore, phosphomimetic ubiquitin accelerates discharge of the thioester conjugate formed by UBCH7 (also known as UBE2L3) and ubiquitin (UBCH7~ubiquitin) in the presence of parkin** ***in vitro*****, indicating that it acts allosterically. The phosphorylation-dependent interaction between ubiquitin and parkin suggests that phosphorylated ubiquitin unlocks autoinhibition of the catalytic cysteine. Our results show that PINK1-dependent phosphorylation of both parkin and ubiquitin is sufficient for full activation of parkin E3 activity. These findings demonstrate that phosphorylated ubiquitin is a parkin activator.**

Dysfunction of PINK1 or parkin seems to cause an accumulation of low-quality depolarized mitochondria and production of excessive reactive oxygen species (ROS), which trigger familial Parkinsonism[3–5]. One of the most poorly understood events in PINK1- and parkin-mediated mitochondrial quality control is how the E3 activity of parkin is accelerated by damaged mitochondria. The simplest model is that PINK1-dependent phosphorylation of parkin accelerates its enzymatic activity. Indeed, parkin is phosphorylated at Ser 65 in a PINK1-dependent manner[13–15]. Furthermore, a phosphorylation-deficient mutation (Ser65Ala) of parkin hindered formation of the ubiquitin-ester intermediate necessary for parkin activation[15]. However, the requirement of PINK1 for parkin activation was not bypassed by the phosphomimetic parkin (Ser65Glu) (the mutation did not make PINK1 dispensable). We thus speculated that parkin is not the sole PINK1 substrate and that phosphorylation of other PINK1 substrate(s) is imperative for parkin activation.

The structure of the amino-terminal parkin UBL (ubiquitin-like) domain resembles that of ubiquitin, and Ser 65 is conserved in both proteins (Extended Data Fig. 1a). Moreover, physical interactions between parkin and ubiquitin have been suggested[16,17]. We therefore examined whether ubiquitin is phosphorylated by PINK1. To detect a phosphorylated ubiquitin, we performed phosphate-affinity (Phos-tag) PAGE in which the phosphorylated ubiquitin can be easily distinguished from the non-phosphorylated form as a slower migrating band[18]. When PINK1-expressing HeLa-cell lysates treated with the protonophore carbonyl cyanide 3-chlorophenylhydrazone (CCCP) were subjected to Phos-tag PAGE, one retarded-mobility form of ubiquitin was specifically observed in the CCCP-treated cell lysate (Fig. 1a). When recombinant ubiquitin and ubiquitin with small N-terminal epitope tags were incubated with isolated mitochondria from CCCP-treated or untreated cells, and then subjected to Phos-tag PAGE (Fig. 1b and Extended Data Fig. 1b), ubiquitin phosphorylation was specifically observed in the reaction containing CCCP-pretreated mitochondria (Fig. 1b, lanes 2, 4, 6). In contrast, the small ubiquitin-related modifier-1 (SUMO-1) protein was not phosphorylated by depolarized mitochondria (Extended Data Fig. 1c), suggesting that phosphorylation of ubiquitin was specific.

To determine the phosphorylation site, the phosphorylated ubiquitin was trypsinized and subjected to liquid chromatography tandem mass spectrometry (LC-MS/MS) analysis. Two phosphorylated ubiquitin peptides, 55–72 (TLSDYNIQKEpSTLHLVLR) and 64–72 (EpSTLHLVLR) were identified with high confidence, suggesting Ser 65 phosphorylation (Extended Data Fig. 1d). Indeed, mutation of Ser 65 prevents ubiquitin phosphorylation by damaged mitochondria *in vitro* (Fig. 1c and Extended Data Fig. 1e) and following protonophore treatment in cells (Fig. 1d and Extended Data Fig. 1f). Next, the absolute levels of phosphorylated ubiquitin of PINK1-expressing HeLa cell lysates (Extended Data Fig. 1g, h) were determined using absolute quantification (AQUA) peptides as standards (Extended Data Table 1). The non-phosphorylated ESTLHLVLR peptide derived from endogenous ubiquitin was detected both in the presence and absence of CCCP, whereas the Ser 65 phosphopeptide (EpSTLH LVLR) was only detected in CCCP-pretreated cells (Fig. 1e and Extended Data Fig. 1i). Absolute quantification revealed that approximately 3% of total endogenous ubiquitin is phosphorylated in PINK1-expressing cells following a decrease in mitochondrial membrane potential ($\Delta\Psi m$).

We next investigated whether PINK1 is required for ubiquitin phosphorylation. When mitochondria derived from *PINK1*-knockout (*PINK1*$^{-/-}$) mouse embryonic fibroblasts (MEFs)[19] were used (Fig. 2a and Extended Data Fig. 2a), ubiquitin phosphorylation was completely impeded even following CCCP pretreatment (Fig. 2a, lane 2). Wild-type PINK1 activated by CCCP treatment[20,21] complemented the phosphorylation of ubiquitin (Fig. 2a, lane 4), whereas PINK1 mutants with decreased kinase

[1]Laboratory of Protein Metabolism, Tokyo Metropolitan Institute of Medical Science, Setagaya-ku, Tokyo 156-8506, Japan. [2]Graduate School of Frontier Sciences, The University of Tokyo, Kashiwa, Chiba 277-8561, Japan. [3]Division of Cell Signaling, Fujii Memorial Institute of Medical Sciences, The University of Tokushima, Tokushima 770-8503, Japan. [4]Research Center for Materials Science, Nagoya University, Nagoya, Aichi 464-8602, Japan. [5]Graduate School of Agriculture, Shizuoka University, 836 Ohya, Shizuoka 422-8529, Japan. [6]Molecular Profiling Research Center for Drug Discovery, National Institute of Advanced Industrial Science and Technology, 2-4-7 Aomi, Koto-ku, Tokyo 135-0064, Japan. [7]JST-CREST/Department of Chemistry, Graduate School of Science, Nagoya University, Chikusa-ku, Nagoya 464-8602, Japan. [8]JST-CREST/Faculty of Life Sciences, Kyoto Sangyo University, Kamigamo-motoyama, Kita-ku, Kyoto 603-8555, Japan. [9]McGill Parkinson Program, Department of Neurology and Neurosurgery, Montreal Neurological Institute and Hospital, McGill University, Montréal, Québec H3A 2B4, Canada. [10]Department of Pharmacology & Therapeutics, McGill University, Montréal, Québec H3G 1Y6, Canada. [11]Protein Metabolism Project, Tokyo Metropolitan Institute of Medical Science, Setagaya-ku, Tokyo 156-8506, Japan.

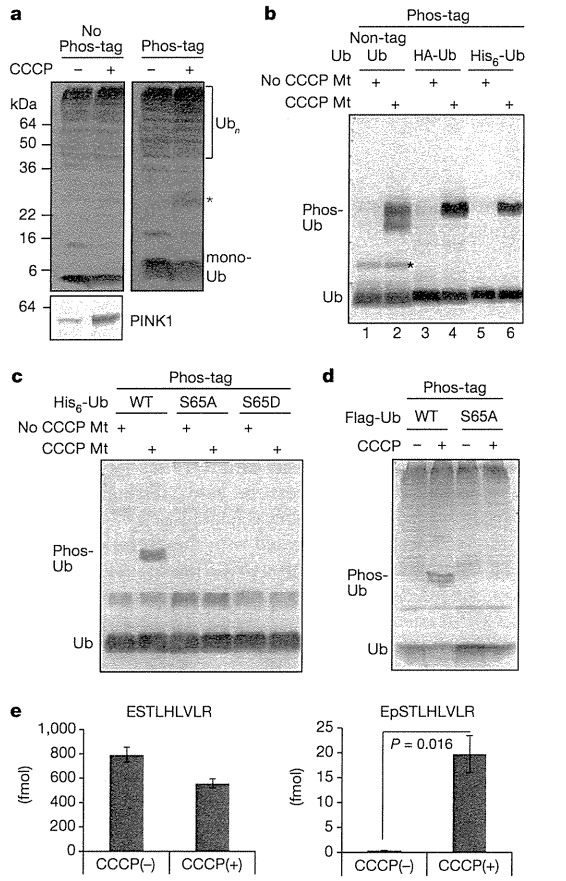

Figure 1 | Ubiquitin Ser 65 is phosphorylated when $\Delta\Psi$m is decreased. **a**, HeLa cells stably expressing PINK1 were treated with protonophore (CCCP) followed by Phos-tag PAGE and immunoblot analysis with an anti-ubiquitin (Ub) antibody. Red asterisk, phosphorylated ubiquitin. Ub_n, ubiquitinated proteins. **b**, Recombinant ubiquitin was phosphorylated by depolarized mitochondria prepared from PINK1-expressing HeLa cells. Black asterisk, cross-reacting band; HA, haemagglutinin; His_6, tandem repeat (×6) of His residues; Phos-Ub, phosphorylated ubiquitin; Non-tag Ub, non-tagged ubiquitin. **c**, **d**, Mutation of Ser 65 prevents ubiquitin phosphorylation by depolarized mitochondria *in vitro* (**c**) and following protonophore treatment in cells (**d**). **e**, Absolute quantification of ESTLHLVLR and EpSTLHLVLR peptides in low-molecular-weight fraction of PINK1-expressing cells. Error bars represent mean ± s.e.m. from three experiments. Statistical significance was calculated using a one-tailed paired *t*-test (significant if $P < 0.05$). WT, wild type.

activity (kinase-dead, Ala168Pro, and Gly386Ala)[20] did not support phosphorylation of ubiquitin (Fig. 2a, lanes 6, 8, 10). To demonstrate PINK1-catalysed ubiquitin phosphorylation more convincingly, immunoprecipitated PINK1 (Extended Data Fig. 2b) was tested *in vitro*. Ubiquitin phosphorylation following incubation with the immunoprecipitated PINK1 was equivalent to that of CCCP-pretreated mitochondria (Fig. 2b and Extended Data Fig. 2c). Moreover, when recombinant ubiquitin was incubated with immunoprecipitated PINK1 and [γ-^{32}P]ATP, incorporation of ^{32}P was detected in the recombinant wild-type ubiquitin (Fig. 2c, lane 2) but not the Ser65Ala ubiquitin mutant (Fig. 2c, lane 4). Taken together, these results demonstrate that PINK1 can phosphorylate ubiquitin at Ser 65. Because the data presented above were derived from PINK1-overproducing cells, we next quantified ubiquitin phosphorylation in intact HeLa cells (Fig. 2d and Extended Data Fig. 3) and found that 0.05% of total endogenous ubiquitin is phosphorylated. Although the absolute level was very low, given the pleiotropic functions of ubiquitin, such a small fraction might be a significant pool dedicated to the PINK1-mediated

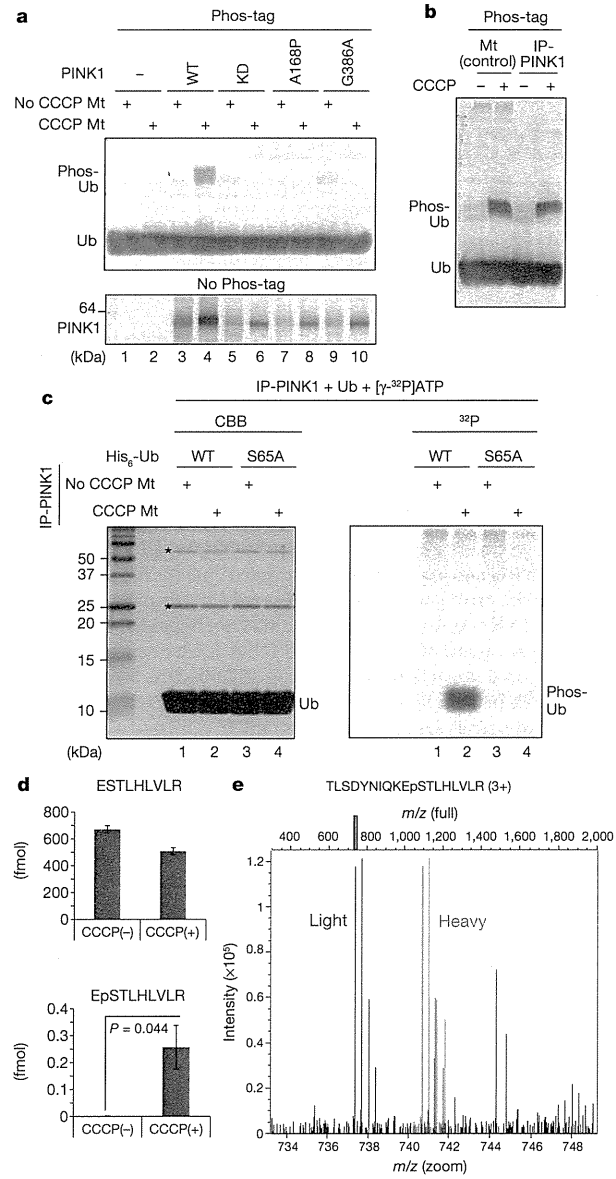

Figure 2 | PINK1 phosphorylates ubiquitin. **a**, Active PINK1 is essential for ubiquitin phosphorylation *in vitro*. Mitochondria isolated from *PINK1*-knockout (*PINK1*$^{-/-}$) mouse embryonic fibroblasts (MEFs) transfected with wild-type and mutant PINK1 were used. **b**, Immunoprecipitated PINK1 (IP-PINK1) can phosphorylate ubiquitin *in vitro* to the same level as depolarized mitochondria. **c**, Ubiquitin was labelled with ^{32}P by IP-PINK1 prepared from CCCP-treated mitochondria, whereas the ubiquitin(Ser65Ala) mutant was not. Asterisks, heavy and light chains of immunoglobulin. **d**, Absolute quantification of endogenous phosphorylated ubiquitin in intact HeLa cells. Statistical analysis was performed as in Fig. 1e. **e**, Precursor $(M + 3H)^{3+}$ spectrum of the peptide harbouring phosphorylated Ser 65. The mass spectrometry peaks are shown in blue, and the orange bar indicates the position of the precursor. The theoretical position of the heavy precursor peptide is shown in transparent red.

activation of parkin. We tested further the dependency on endogenous PINK1. HeLa cells grown in light or heavy SILAC (stable isotope labeling using amino acids in cell culture) media were treated with non-target or *PINK1* siRNA, respectively (Extended Data Fig. 2d), and then subjected to LC-MS/MS analysis. Phosphorylated Ser 65 peptide was present in control siRNA cells (Fig. 2e, peak identified as 'light') but absent

in *PINK1* siRNA (siPINK1) cells (peak identified as 'heavy'), indicating endogenous PINK1 phosphorylated ubiquitin at Ser 65 in intact cells.

We next investigated the role of phosphorylated ubiquitin. If ubiquitin is the genuine PINK1 substrate, a phosphomimetic ubiquitin mutant would be expected to bypass the PINK1-dependency of parkin activation[8] or parkin recruitment onto depolarized mitochondria[8–12]. To monitor the E3 activity of parkin, autoubiquitination of green fluorescent protein (GFP)-tagged parkin (GFP–parkin) was used as an index[8]. In our first trial, expression of phosphomimetic ubiquitin(Ser65Asp) mutants led to neither mitochondrial localization (Fig. 3a, b) nor autoubiquitination of GFP–parkin (Fig. 3c, lane3). However, the CCCP treatment control triggered both mitochondrial localization (not shown) and autoubiquitination (Fig. 3c, lanes 4–6) of GFP–parkin. Because PINK1 also phosphorylates parkin[13–15], we used a phosphomimetic parkin mutant, parkin(Ser65Glu)[15], in case both phosphorylation events are necessary. Cytoplasmic localization of GFP–parkin(Ser65Glu) remained unchanged following co-expression with the ubiquitin(Ser65Asp) (Fig. 3d, e), whereas CCCP treatment stimulated translocation of GFP–parkin(Ser65Glu) to mitochondria (not shown). In sharp contrast, phosphomimetic ubiquitin (Ser65Asp) localized in cytoplasm (Extended Data Fig. 4a) promoted autoubiquitination of GFP–parkin(Ser65Glu) even in the absence of CCCP treatment (Fig. 3f, lane 3). Moreover, overproduction of phosphorylation-deficient ubiquitin(Ser65Ala) delayed CCCP-triggered parkin activation as compared with phosphorylatable wild-type ubiquitin, suggesting that the unphosphorylatable ubiquitin mutant competed with endogenous ubiquitin and thus exerted a dominant-negative effect (Fig. 3g).

Recently, it was noted that the parkin Trp403Ala mutation weakened autoinhibition and accelerated E3 activity[22]. When GFP–parkin (Trp403Ala) was co-expressed with ubiquitin(Ser65Asp), its autoubiquitination was also observed even without CCCP treatment (Fig. 3h, lane 3). These results suggest phosphorylated ubiquitin functions as a parkin activator; otherwise parkin might preferentially use phosphorylated ubiquitin for conjugation. To investigate this, we mutated the carboxy-terminal diglycine motif of ubiquitin(Ser65Asp), which is crucial for formation of the thioester intermediate during the ubiquitination cascade. As shown in Fig. 3i, phosphomimetic ubiquitin with the diglycine mutations (Gly75Val/Gly76Val or Gly75Ala/Gly76Ala) still stimulated the E3 activity of GFP–parkin(Ser65Glu) and GFP–parkin(Trp403Ala) (Fig. 3i, lanes 5, 6, 11, 12; endogenous ubiquitin was conjugated). Moreover, parkin catalyses conjugation of phosphorylation-deficient ubiquitin(Ser65Ala) to depolarized mitochondria following CCCP treatment (Fig. 3j, k), indicating that parkin does not exclusively use phosphorylated ubiquitin for ubiquitination. Nevertheless, phosphomimetic ubiquitin could be recruited to mitochondria and conjugated to mitofusin-2 (Extended Data Fig. 4b, c) in a CCCP-dependent manner. Thus, parkin conjugates both unphosphorylated and phosphorylated ubiquitin to substrates.

We confirmed further the aforementioned results in a cell-free assay using GFP–parkin and purified mitochondria[15,23]. Autoubiquitination of GFP–parkin in intact cell extracts was specifically observed when incubated with CCCP-pretreated mitochondria[15,23]. In contrast, autoubiquitination of GFP–parkin mutants harbouring the Ser65Glu or Trp403Ala mutations was clearly observed when incubated with recombinant phosphomimetic ubiquitin(Ser65Asp) in the absence of depolarized mitochondria (Fig. 4a, lanes 12, 18). Wild-type ubiquitin and the phosphorylation-deficient Ser65Ala mutant did not support autoubiquitination of parkin(Ser65Glu) or parkin(Trp403Ala) (lanes 7–10, 13–16), and ubiquitin(Ser65Asp) did not accelerate autoubiquitination of wild-type GFP–parkin (lane 6). To rule out the possible effect of PINK1 contamination, we repeated the experiments using GFP–parkin prepared from *PINK1*$^{-/-}$ MEFs. Autoubiquitination of both Ser65Glu and Trp403Ala mutants of GFP–parkin were again observed (Fig. 4b), further supporting the idea that phosphomimetic ubiquitin makes PINK1 dispensable for phosphomimetic parkin activation.

We next examined directly whether phosphorylated ubiquitin (not phosphomimetic ubiquitin) activated parkin. Ubiquitin was phosphorylated by incubation with depolarized mitochondria, then subjected to

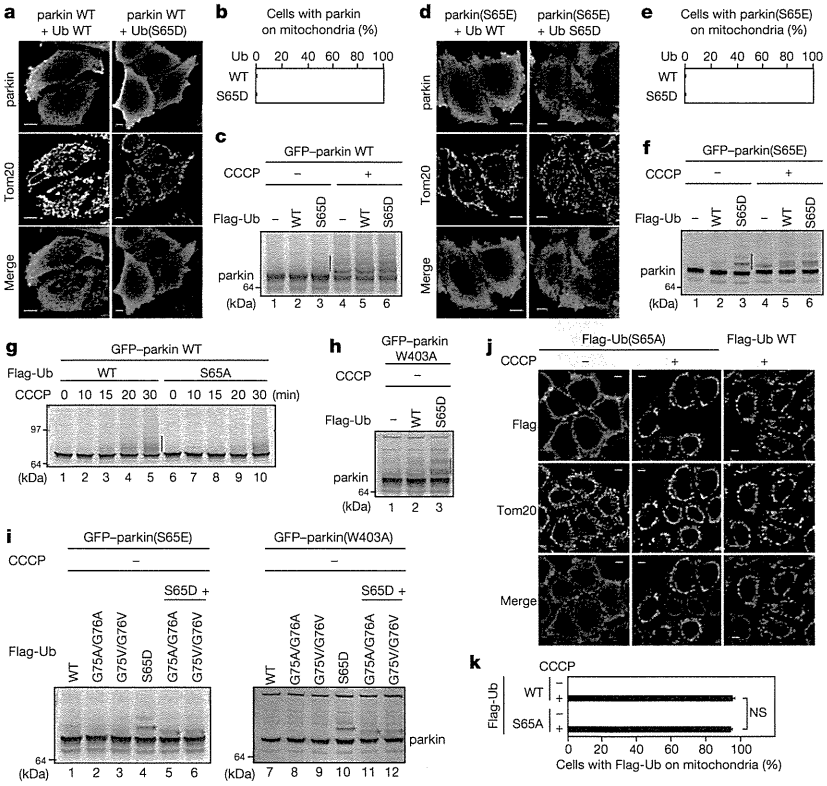

Figure 3 | Phosphomimetic ubiquitin activates phosphomimetic parkin. **a**, Cytoplasmic localization of WT parkin co-expressed with WT or phosphomimetic ubiquitin(Ser65Asp). Scale bars indicate 10 μm. **b**, The rate of mitochondrial parkin localization was 0% when calculated in 100 cells across three experiments. **c**, Autoubiquitination of GFP–parkin was not observed by co-expression of phosphomimetic ubiquitin (red vertical bars). **d**, **e**, Cytoplasmic localization of the phosphomimetic parkin(Ser65Glu) mutant co-expressed with WT or phosphomimetic ubiquitin. Immunocytochemistry (**d**) and statistical analysis (**e**) were performed as in **a** and **b**. **f**, Autoubiquitination of phosphomimetic GFP–parkin(Ser65Glu) was observed following co-expression of phosphomimetic ubiquitin(Ser65Asp) even in the absence of CCCP treatment (lane 3). **g**, Co-expression of phosphorylation-deficient ubiquitin(Ser65Ala) mutant delayed CCCP-dependent activation of WT parkin. **h**, Phosphomimetic ubiquitin(Ser65Asp) induced autoubiquitination of GFP–parkin(Trp403Ala). **i**, The C-terminal diglycine motif (GG) is dispensable for parkin activation. Red asterisks, autoubiquitination of the GFP–parkin(Ser65Glu) and GFP–parkin(Trp403Ala) mutants. **j**, Mitochondrial localization of phosphorylation-deficient ubiquitin(Ser65Ala) mediated by parkin, following a decrease in $\Delta\Psi$m. **k**, The rate of cells with Flag-Ub on mitochondria was calculated as a percentage using 100 cells across three experiments. Error bars represent the mean ± s.e.m. NS, not significant ($P > 0.05$) in a one-tailed Student's *t*-test.

ultracentrifugation to deplete mitochondria, and finally treated at 90 °C for 10 min. Ubiquitin is a rare heat-stable protein and resistant to 90 °C treatment[24], whereas any contaminating PINK1 would be inactivated under these conditions (Extended Data Fig. 5). The phosphorylated ubiquitin induced clear autoubiquitination of GFP–parkin(Ser65Glu) and GFP–parkin(Trp403Ala) (Fig. 4c, lanes 4 and 6), indicating that phosphorylated ubiquitin activates parkin *in vitro*. Similarly, when ubiquitin harboring the Gly75Ala/Gly76Ala mutation was phosphorylated beforehand and incubated with a GFP–parkin(Ser65Glu)-containing lysate, autoubiquitination of GFP–parkin(Ser65Glu) was observed (Fig. 4d, lane 6; note that the conjugation-competent endogenous ubiquitin is supplied in the parkin-containing lysate), confirming that phosphorylated ubiquitin activates parkin(Ser65Glu) independent of its conjugation (Fig. 3i), whereas non-phosphorylated ubiquitin(Gly75Ala/Gly76Ala) does not promote autoubiquitination (Fig. 4d, lane 4).

To confirm the dependency of parkin activation on ubiquitin phosphorylation, we used a yeast system in which all of the genomic-ubiquitin genes are disrupted, the fused ribosomal proteins (L40 and S31) are complemented, and ubiquitin is expressed from a plasmid[25]. We introduced the Ser65Ala mutation into the yeast ubiquitin plasmid and co-expressed it with PINK1 and GFP–parkin (note that yeast lack PINK1 and parkin homologues). GFP–parkin in yeast cells harbouring wild-type ubiquitin underwent autoubiquitination when co-expressed with wild-type PINK1, but lacked the modification when expressed with a kinase-dead PINK1 mutation or pathogenic parkin mutations (Extended Data Fig. 6). In contrast, even when co-expressed with wild-type PINK1, GFP–parkin did not show this modification in yeast only expressing the mutant ubiquitin(Ser65Ala) (Fig. 4e). Taken together, the results obtained using this stringent heterologous cellular system argue strongly that ubiquitin phosphorylation at Ser 65 is indeed essential for parkin activation.

Finally, we sought to define the molecular mechanism by which phosphorylated ubiquitin activates parkin. We confirmed that phosphorylated ubiquitin was charged on UBCH7 as readily as non-phosphorylated ubiquitin (Fig. 4f and Extended Data Fig. 7a), indicating a similar efficiency

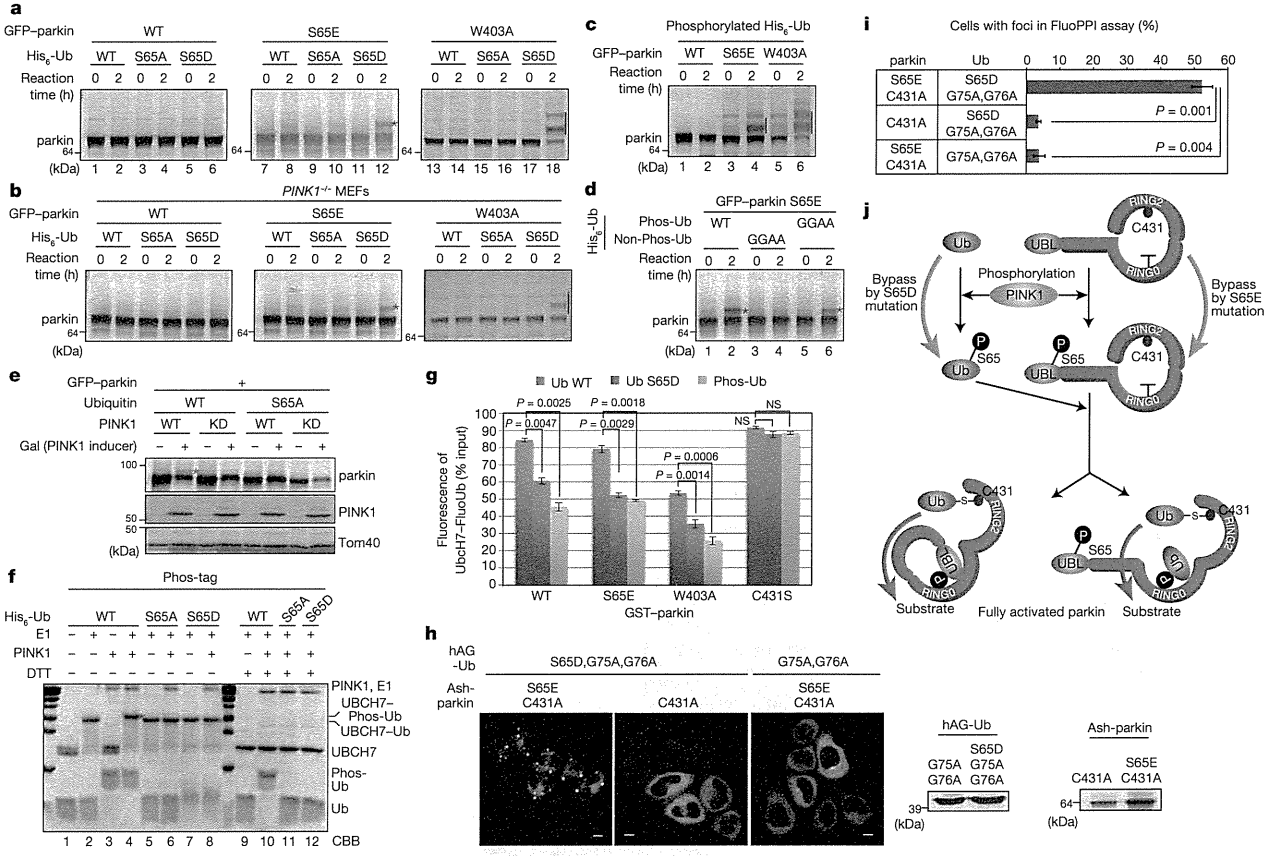

Figure 4 | Molecular mechanism underlying parkin activation by phosphorylated ubiquitin. **a**, **b**, Recombinant phosphomimetic ubiquitin(Ser65Asp) activates GFP–parkin(Ser65Glu) and GFP–parkin(Trp403Ala) mutants prepared from HeLa cells (**a**) and *PINK1*$^{-/-}$ MEFs (**b**). **c**, Recombinant phosphorylated ubiquitin activated Ser65Glu and Trp403Ala GFP–parkin from mitochondria-intact cells. **d**, Phosphorylated ubiquitin(Gly75Ala/Gly76Ala) that cannot be conjugated still promoted autoubiquitination of parkin(Ser65Glu). Non-Phos-Ub, non-phosphorylated ubiquitin; Phos-Ub, phosphorylated ubiquitin. **e**, Mitochondrial-localized PINK1 in yeast cells harbouring WT ubiquitin activates parkin, but parkin is not activated when ubiquitin is replaced with the Ser65Ala mutant. Red asterisks and red vertical bars in **a**–**e** indicate autoubiquitination of GFP–parkin. **f**, UBCH7 can be charged with phosphorylated Ub, as seen in the shift observed in UBCH7~Phos-Ub (lane 4, red asterisk indicates thioester-linked ubiquitination), or with ubiquitin(Ser65Asp) (lanes 7, 8). CBB, Coomassie Brilliant Blue; DTT, dithiothreitol. **g**, phosphomimetic and phosphorylated ubiquitin accelerates discharging of UBCH7~ubiquitin in the presence of catalytically active parkin *in vitro*. Error bars represent the mean ± s.d. values in three experiments, and statistical significance was calculated using a one-tailed paired *t*-test. NS, not significant ($P > 0.05$). **h**, FluoPPI assay revealed a physical interaction between phosphomimetic parkin and phosphomimetic ubiquitin. A Cys431Ala mutation of parkin and a Gly75Ala/Gly76Ala mutation of ubiquitin prevented a ubiquitination-derived pseudo-positive signal. hAG-Ub, hAG (homo tetramer Azami-GFP)-tagged ubiquitin; Ash-parkin, Ash (homo-oligomerized protein assembly helper)-tagged parkin. Scale bars indicate 10 μm. **i**, Foci-containing cells were calculated in 100 cells across three experiments. Error bars represent the mean ± s.e.m. and statistical significance was calculated using a one-tailed paired *t*-test. **j**, A model for parkin activation. PINK1 activates latent parkin via two phosphorylation steps at Ser 65 in both the parkin UBL domain and ubiquitin, which de-repress the RING0 domain and relieve the catalytic cysteine (Cys 431). All experiments were repeated twice with similar results.

of conjugation by E2. We then examined whether phosphomimetic and phosphorylated ubiquitin accelerates discharge of UBCH7~unmodified ubiquitin (UBCH7 harbouring thioester-linked unmodified ubiquitin) in the presence of parkin *in vitro* (note that the reaction does not contain ATP, thus free phosphorylated ubiquitin cannot enter into the conjugation pathway). Both phosphomimetic and phosphorylated ubiquitin accelerates discharge of ubiquitin from UBCH7~ubiquitin depending on the presence of catalytic cysteine (Cys 431) of parkin, revealing that the activation mechanism is strictly allosteric (Fig. 4g and Extended Data Fig. 7b). We next examined whether phosphorylated ubiquitin interacts physically with parkin. Using the FluoPPI (fluorescent-based technology detecting protein–protein interactions) technique, in which protein–protein interactions are detectable as foci formation in living cells, we demonstrated a clear interaction between parkin and ubiquitin in cells. Importantly, parkin with an intact UBL domain failed to interact with phosphomimetic ubiquitin, whereas parkin with a phosphomimetic (Ser65Glu) UBL mutation was able to interact (Figs. 4h, i). This result suggests that the interaction between parkin and phosphorylated ubiquitin competes with the intact parkin UBL domain, whereas phosphorylation of the UBL domain releases this inhibitory effect. Recently, the structure of parkin[22,26–28] revealed that the RING0 domain occludes the catalytic cysteine (Cys 431). To gain further insight into the mechanism, we used computational modelling to generate two structural models that support binding of phosphorylated ubiquitin or phosphorylated UBL domain facilitates accessibility to Cys 431 (Extended Data Fig. 8). Because phosphorylation at both sites is required for parkin activation (Fig. 3), either of these conformations might be an intermediate to the other. Based on our combined results and the autoinhibitory effect of the UBL domain[16], we speculate that phosphorylation of both ubiquitin and the UBL domain unlock repression of the catalytic cysteine by the RING0 domain, thereby converting parkin to its fully-active form (Fig. 4j).

In the present study, we demonstrate—to our knowledge, for the first time—that parkin activation in response to mitochondrial damage proceeds following ubiquitin phosphorylation by PINK1. The E3 activity of parkin is usually repressed via autoinhibition[8,16,22,26,27] but is specifically liberated by PINK1 in a unique two-step phosphorylation-dependent manner: one step is the phosphorylation of the UBL domain of parkin[13–15], and the other step is, unexpectedly, phosphorylation of ubiquitin (determined in this work). As mitochondrial dysfunction has long been associated with sporadic Parkinson's disease[29], a complete understanding of the molecular mechanism underlying parkin activation is expected to clarify the pathogenesis of not only hereditary but also sporadic forms of Parkinson's disease. Moreover, although thousands of papers studying ubiquitin have been published, this work is the first, to our knowledge, to reveal ubiquitin phosphorylation and its significance.

METHODS SUMMARY

Immunoprecipitation of PINK1 (ref. 21), Phos-tag PAGE[15,20], *in vitro* ubiquitination of GFP–parkin on depolarized mitochondria[15,23], charging and discharging assay[22], and mass spectrometric analyses[15,20,30] were performed as reported previously. Detailed procedures are available in the Methods (online).

Online Content Any additional Methods, Extended Data display items and Source Data are available in the online version of the paper; references unique to these sections appear only in the online paper.

Received 29 January; accepted 23 April 2014.
Published online 30 April 2014.

1. Kitada, T. *et al.* Mutations in the parkin gene cause autosomal recessive juvenile parkinsonism. *Nature* **392,** 605–608 (1998).
2. Valente, E. M. *et al.* Hereditary early-onset Parkinson's disease caused by mutations in PINK1. *Science* **304,** 1158–1160 (2004).
3. Narendra, D., Walker, J. E. & Youle, R. Mitochondrial quality control mediated by PINK1 and Parkin: links to Parkinsonism. *Cold Spring Harb. Perspect. Biol.* **4,** a011338 (2012).
4. Corti, O., Lesage, S. & Brice, A. What genetics tells us about the causes and mechanisms of Parkinson's disease. *Physiol. Rev.* **91,** 1161–1218 (2011).
5. Exner, N., Lutz, A. K., Haass, C. & Winklhofer, K. F. Mitochondrial dysfunction in Parkinson's disease: molecular mechanisms and pathophysiological consequences. *EMBO J.* **31,** 3038–3062 (2012).
6. Clark, I. E. *et al. Drosophila pink1* is required for mitochondrial function and interacts genetically with parkin. *Nature* **441,** 1162–1166 (2006).
7. Park, J. *et al.* Mitochondrial dysfunction in *Drosophila PINK1* mutants is complemented by *parkin*. *Nature* **441,** 1157–1161 (2006).
8. Matsuda, N. *et al.* PINK1 stabilized by mitochondrial depolarization recruits Parkin to damaged mitochondria and activates latent Parkin for mitophagy. *J. Cell Biol.* **189,** 211–221 (2010).
9. Narendra, D. P. *et al.* PINK1 is selectively stabilized on impaired mitochondria to activate Parkin. *PLoS Biol.* **8,** e1000298 (2010).
10. Geisler, S. *et al.* PINK1/Parkin-mediated mitophagy is dependent on VDAC1 and p62/SQSTM1. *Nature Cell Biol.* **12,** 119–131 (2010).
11. Vives-Bauza, C. *et al.* PINK1-dependent recruitment of Parkin to mitochondria in mitophagy. *Proc. Natl Acad. Sci. USA* **107,** 378–383 (2010).
12. Ziviani, E., Tao, R. N. & Whitworth, A. J. Drosophila parkin requires PINK1 for mitochondrial translocation and ubiquitinates mitofusin. *Proc. Natl Acad. Sci. USA* **107,** 5018–5023 (2010).
13. Kondapalli, C. *et al.* PINK1 is activated by mitochondrial membrane potential depolarization and stimulates Parkin E3 ligase activity by phosphorylating Serine 65. *Open Biol.* **2,** 120080 (2012).
14. Shiba-Fukushima, K. *et al.* PINK1-mediated phosphorylation of the Parkin ubiquitin-like domain primes mitochondrial translocation of Parkin and regulates mitophagy. *Sci. Rep.* **2,** 1002 (2012).
15. Iguchi, M. *et al.* Parkin-catalyzed ubiquitin-ester transfer is triggered by PINK1-dependent phosphorylation. *J. Biol. Chem.* **288,** 22019–22032 (2013).
16. Chaugule, V. K. *et al.* Autoregulation of Parkin activity through its ubiquitin-like domain. *EMBO J.* **30,** 2853–2867 (2011).
17. Zheng, X. & Hunter, T. Parkin mitochondrial translocation is achieved through a novel catalytic activity coupled mechanism. *Cell Res.* **23,** 886–897 (2013).
18. Kinoshita, E., Kinoshita-Kikuta, E., Takiyama, K. & Koike, T. Phosphate-binding tag, a new tool to visualize phosphorylated proteins. *Mol. Cell. Proteom.* **5,** 749–757 (2006).
19. Gautier, C. A., Kitada, T. & Shen, J. Loss of PINK1 causes mitochondrial functional defects and increased sensitivity to oxidative stress. *Proc. Natl Acad. Sci. USA* **105,** 11364–11369 (2008).
20. Okatsu, K. *et al.* PINK1 autophosphorylation upon membrane potential dissipation is essential for Parkin recruitment to damaged mitochondria. *Nature Commun.* **3,** 1016 (2012).
21. Okatsu, K. *et al.* A dimeric PINK1-containing complex on depolarized mitochondria stimulates Parkin recruitment. *J. Biol. Chem.* **288,** 36372–36384 (2013).
22. Trempe, J. F. *et al.* Structure of parkin reveals mechanisms for ubiquitin ligase activation. *Science* **340,** 1451–1455 (2013).
23. Lazarou, M. *et al.* PINK1 drives Parkin self-association and HECT-like E3 activity upstream of mitochondrial binding. *J. Cell Biol.* **200,** 163–172 (2013).
24. Ciehanover, A., Hod, Y. & Hershko, A. A heat-stable polypeptide component of an ATP-dependent proteolytic system from reticulocytes. 1978. *Biochem. Biophys. Res. Commun.* **81,** 1100–1105 (1978).
25. Spence, J., Sadis, S., Haas, A. L. & Finley, D. A ubiquitin mutant with specific defects in DNA repair and multiubiquitination. *Mol. Cell. Biol.* **15,** 1265–1273 (1995).
26. Riley, B. E. *et al.* Structure and function of Parkin E3 ubiquitin ligase reveals aspects of RING and HECT ligases. *Nature Commun.* **4,** 1982 (2013).
27. Wauer, T. & Komander, D. Structure of the human Parkin ligase domain in an autoinhibited state. *EMBO J.* **32,** 2099–2112 (2013).
28. Spratt, D. E. *et al.* A molecular explanation for the recessive nature of parkin-linked Parkinson's disease. *Nature Commun.* **4,** 1983 (2013).
29. Schapira, A. H. Complex I: inhibitors, inhibition and neurodegeneration. *Exp. Neurol.* **224,** 331–335 (2010).
30. Tsuchiya, H., Tanaka, K. & Saeki, Y. The parallel reaction monitoring method contributes to a highly sensitive polyubiquitin chain quantification. *Biochem. Biophys. Res. Commun.* **436,** 223–229 (2013).

Acknowledgements This work was supported by JSPS KAKENHI grant numbers 23687018 (to N.M.), 23-6061 (to K.O.), 21000012 (to K.T.), 24657072 and 22227003 (to Y.T. and T.E.); MEXT KAKENHI grant numbers 24111557 and 25112522 (to N.M.), 24112008 (to Y.S.); the Tomizawa Jun-ichi and Keiko Fund (to N.M.); JST CREST (to T.E.); Platform for Drug Discovery, Informatics, and Structural Life Science from MEXT (to T.H.); startup funds from McGill University and the GRASP from the FRSQ (to J.-F.T.); an Operating Grant from the CIHR and a Chercheur National Award from the FRSQ (to E.A.F.); and the Takeda Science Foundation (to H.K., K.T. and N.M.). We thank N. Croteau and S. Rasool for technical assistance, T. Ueno for anti-FoF1 antibody, and D. Finley for yeast strain SUB328.

Author Contributions F.K., K.O., H.K., E.G., J.-F.T. and M.K. carried out biochemical and immunoblot experiments. T.H. performed computational modelling. Y.T., Y.K., Y.S. and T.E. performed yeast experiments. F.K., E.G. and M.K. performed immunocytochemistry. F.K., H.T., H.Y., J.-F.T., E.A.F. and Y.S. performed mass spectrometric analysis. K.T. and N.M. designed the research and analysed the data. N.M. wrote the manuscript with help and supervision from K.T. All authors contributed to data analysis and preparation of the manuscript.

Author Information Reprints and permissions information is available at www.nature.com/reprints. The authors declare no competing financial interests. Readers are welcome to comment on the online version of the paper. Correspondence and requests for materials should be addressed to Noriyuki Matsuda (matsuda-nr@igakuken.or.jp) and Keiji Tanaka (tanaka-kj@igakuken.or.jp).

Available online at www.sciencedirect.com
ScienceDirect
www.elsevier.com/locate/brainres
Brain Research

Research Report

Unique nuclear vacuoles in the motor neurons of conditional ADAR2-knockout mice

Shoichi Sasaki[a,*], *Takenari Yamashita*[b,c], *Takuto Hideyama*[b], *Shin Kwak*[b,c,d]

[a]*Department of Neurology, Tokyo Women's Medical University, 8-1 Kawada-cho, Shinjuku-ku, Tokyo 162-8666, Japan*
[b]*Department of Neurology, Graduate School of Medicine, University of Tokyo, Japan*
[c]*Division of Clinical Biotechnology, Center for Disease Biology and Integrative Medicine, Graduate School of Medicine, University of Tokyo, Japan*
[d]*Clinical Research Center for Medicine, International University of Health and Welfare, Japan*

ARTICLE INFO

Article history:
Accepted 7 January 2014
Available online 15 January 2014

Keywords:
Amyotrophic lateral sclerosis
Motor neuron disease
AMPA receptor
GluA2
RNA editing
Conditional ADAR2-knockout mouse
Nuclear vacuole
Pathology
Electron microscopy

ABSTRACT

A reduction in adenosine deaminase acting on RNA 2 (ADAR2) activity causes the death of spinal motor neurons specifically via the GluA2 Q/R site-RNA editing failure in sporadic amyotrophic lateral sclerosis (ALS). We studied, over time, the spinal cords of ADAR2-knockout mice, which are the mechanistic model mice for sporadic ALS, using homozygous ADAR2$^{flox/flox}$/VAChT-Cre.Fast (AR2), homozygous ADAR2$^{flox/flox}$/VAChT-Cre.Slow (AR2Slow), and heterozygous ADAR2$^{flox/+}$/VAChT-Cre.Fast (AR2H) mice. The conditional ADAR2-knockout mice were divided into 3 groups by stage: presymptomatic (AR2H mice), early symptomatic (AR2 mice, AR2H mice) and late symptomatic (AR2Slow mice). Light-microscopically, some motor neurons in AR2 and AR2H mice (presymptomatic) showed simple neuronal atrophy and astrogliosis, and AR2H (early symptomatic) and AR2Slow mice often showed vacuoles predominantly in motor neurons. The number of vacuole-bearing anterior horn neurons decreased with the loss of anterior horn neurons in AR2H mice after 40 weeks of age. Electron-microscopically, in AR2 mice, while the cytoplasm of normal-looking motor neurons was almost always normal-appearing, the interior of dendrites was frequently loose and disorganized. In AR2H and AR2Slow mice, large vacuoles without a limiting membrane were observed in the anterior horns, preferentially in the nuclei of motor neurons, astrocytes and oligodendrocytes. Nuclear vacuoles were not observed in AR2res (ADAR2$^{flox/flox}$/VAChT-Cre.Fast/GluR-B$^{R/R}$) mice, in which motor neurons express edited GluA2 in the absence of ADAR2. These findings suggest that ADAR2-reduction is associated with progressive deterioration of nuclear architecture, resulting in vacuolated nuclei due to a Ca^{2+}-permeable AMPA receptor-mediated mechanism.

Abbreviations: ADAR2, adenosine deaminase acting on RNA 2; ALS, amyotrophic lateral sclerosis; AMPA, L-α-amino-3-hydroxy-5-methyl-4-isoxazolepropionic acid; AR2, homozygous ADAR2$^{flox/flox}$/VAChT-Cre.Fast; AR2Slow, homozygous ADAR2$^{flox/flox}$/VAChT-Cre.Slow; AR2H, heterozygous ADAR2$^{flox/+}$/VAChT-Cre.Fast; rER, rough endoplasmic reticulum

*Corresponding author. Fax: +81 3 5269 7324.
E-mail address: ssasaki@nij.twmu.ac.jp (S. Sasaki).

0006-8993/$ - see front matter © 2014 Elsevier B.V. All rights reserved.
http://dx.doi.org/10.1016/j.brainres.2014.01.006

1. Introduction

GluA2, also known as GluR2 or GluR-B, is a subunit of the L-α-amino-3-hydroxy-5-methyl-4-isoxazolepropionic acid (AMPA) receptor, which is a subtype of ionotropic glutamate receptors. The Ca^{2+} conductance of AMPA receptors differs markedly, depending on whether or not the GluA2 subunit is a component of the receptor. The properties of GluA2 are generated post-transcriptionally by a single nucleotide conversion from adenosine (A) to inosine (I) by RNA processing called RNA editing (A-to-I editing) (Yang et al., 1995), during which the glutamine (Q) codon (CAG) is replaced with an arginine (R) codon (CIG; CGG) at the glutamine/arginine (Q/R) site (Seeburg, 2002). Editing at the GluA2 Q/R site in neurons occurs with virtually 100% efficiency throughout life from the embryonic stage. RNA editing at the GluA2 Q/R site is catalyzed by adenosine deaminase acting on RNA 2 (ADAR2) (Melcher et al., 1996). AMPA receptors expressed in mammalian and human neurons are impermeable to Ca^{2+} due to the presence of Q/R site-edited GluA2 in their subunit assembly, whereas those lacking GluA2 in the subunit or those containing Q/R site-unedited GluA2 are Ca^{2+}- permeable (Burnashev et al., 1992; Seeburg et al., 2001). There is strong evidence indicating that an AMPA receptor-mediated excitotoxic mechanism plays a pathogenic role in amyotrophic lateral sclerosis (ALS) and Cu/Zn superoxide dismutase (SOD1)-associated familial ALS model animals (Roshstein et al., 1992; Van Damme et al., 2005). The spinal motor neurons of sporadic ALS patients specifically express Q/R site-unedited GluA2 mRNA. This is in marked contrast to the fact that all GluA2 mRNA are edited at the Q/R site in the motor neurons of control individuals (Kawahara et al., 2004) and patients with motor neuron diseases other than sporadic ALS such as SOD1-associated familial ALS (Kawahara et al., 2006), as well as in the degenerated neurons in other neurodegenerative diseases, including Purkinje cells of patients with spinocerebellar degeneration (Kawahara et al., 2004; Akbarian et al., 1995). Thus, the defect in GluA2 Q/R site-editing is likely to be specific to sporadic ALS spinal motor neurons. Moreover, the expression level of ADAR2 mRNA, which is one of the determinants of GluA2 Q/R site-RNA editing in the human brain (Kawahara et al., 2003), is significantly reduced in the anterior horn (Kawahara and Kwak, 2005; Kwak and Kawahara, 2005) and motor neurons (Hideyama et al., 2012a) of the spinal cord in sporadic ALS patients compared with that of control subjects. That is, a reduction in ADAR2 activity causes the death of motor neurons via a failure to efficiently edit the GluA2 Q/R site in sporadic ALS.

To investigate whether deficient ADAR2 activity plays a pathogenic role in sporadic ALS, we developed genetically modified mice ($ADAR2^{flox/flox}$/VAChT-Cre.Fast mice designated as AR2 mice) in which the ADAR2 gene is conditionally knocked out in the motor neurons, using the Cre/loxP recombination system. We demonstrated that the loss of ADAR2 activity induces the manifestations of motor dysfunction and the slow death of ADAR2-deficient motor neurons in the spinal cord and cranial motor nerve nuclei in mice (Hideyama et al., 2010). Thus, a reduction in ADAR2 activity causes the death of motor neurons specifically via the GluA2 Q/R site editing failure, and this conditional ADAR2-knockout mouse model mimicking patient-derived molecular abnormalities is considered to be more specific to sporadic ALS. Here, we report on the unique nuclear vacuoles in the dying spinal cord motor neurons of homozygous AR2 and heterozygous AR2 mice. Given that these motor neurons undergo slow degeneration, these nuclear vacuoles are the morphological change that is closely relevant to the Ca^{2+}-permeable AMPA receptor-mediated death of motor neurons.

2. Results

The time-dependent changes are illustrated by the proportion of Cre-expressing, and therefore, the proportion of ADAR2-lacking anterior horn cells in the three lines of AR2 mice (Fig. 1). In AR2 and AR2H mice, Cre-mediated ablation of the ADAR2 gene occurred in a progressively larger proportion of motor neurons, and the Cre expression in AR2 mice reached the maximum level (~50% of motor neurons) by postnatal week 5 (Misawa et al., 2003). AR2Slow mice in which the temporal profile of Cre-mediated knockout of the ADAR2 gene was slower, reaching ~50% of motor neurons by eight months of age (Hideyama and Kwak, 2011; Misawa et al., 2003). Cre expression levels were found not to differ between mice heterozygous and those homozygous for the VAChT-Cre.Fast transgene (Misawa et al., 2003). The number of ADAR2-lacking anterior horn cells significantly decreased in AR2 mice after 2 months of age as a result of Cre-dependent knock-out of ADAR2 (Hideyama et al., 2010). AR2res mice show the same Cre expression pattern with targeting of the ADAR2 alleles as AR2 and AR2H mice do because of the VAChT-Cre.Fast transgene, but they express normal Ca^{2+}-impermeable AMPA receptors due to genetically engineered endogenous GluA2 gene encoding Q/R site edited GluA2 (Hideyama et al., 2010; Kask et al., 1998). In this study,

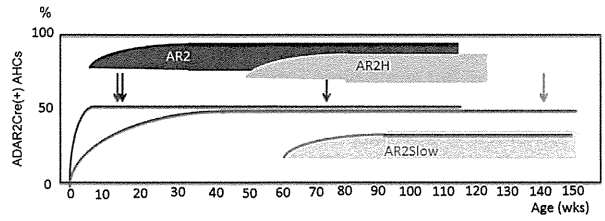

Fig. 1 – A visual overview of AR2 mice strains. Time-dependent changes are illustrated in the proportion of Cre-expressing and ADAR2-lacking anterior horn cells in the three lines of AR2 mice. In AR2 and AR2H mice, Cre-mediated ablation of the $ADAR2^{flox}$ allele occurs in a progressively larger proportion of motor neurons, and the Cre expression in AR2 mice reached the maximum level (~50% of motor neurons) by postnatal week 5. AR2Slow mice in which the temporal profile of Cre-mediated knockout of the ADAR2 gene is slower, reaching ~50% of motor neurons by eight months of age. AR2res mice show a fast transgene pattern. The three shaded areas represent the temporal profile of motor dysfunction. Arrows indicate the weeks of mice investigated, Blue line: VAChT-Cre. Fast transgene (AR2, AR2H and AR2res), Orange line: VAChT-Cre.Slow transgene (AR2Slow), AHCs: anterior horn cells.